nature chemical biology

Article

https://doi.org/10.1038/s41589-024-01748-5

Fucosylation of glycoproteins and glycolipids: opposing roles in cholera intoxication

Received: 8 August 2023

Accepted: 13 September 2024

Published online: 16 October 2024

Check for updates

Atossa C. Ghorashi[1], Andrew Boucher[2], Stephanie A. Archer-Hartmann[3], Dani Zalem[4], Mehrnoush Taherzadeh Ghahfarrokhi[3], Nathan B. Murray[3], Rohit Sai Reddy Konada[1], Xunzhi Zhang[5], Chao Xing[5,6], Susann Teneberg[4], Parastoo Azadi[3], Ulf Yrlid[2] & Jennifer J. Kohler[1]

Cholera toxin (CT) is the etiological agent of cholera. Here we report that multiple classes of fucosylated glycoconjugates function in CT binding and intoxication of intestinal epithelial cells. In Colo205 cells, knockout (KO) of *B3GNT5*, which encodes an enzyme required for synthesis of lacto and neolacto series glycosphingolipids (GSLs), reduces CT binding but sensitizes cells to intoxication. Overexpressing *B3GNT5* to generate more fucosylated GSLs confers protection against intoxication, indicating that fucosylated GSLs act as decoy receptors for CT. KO of *B3GALT5* causes increased production of fucosylated *O*-linked and *N*-linked glycoproteins and leads to increased CT binding and intoxication. KO of *B3GNT5* in *B3GALT5*-KO cells eliminates production of fucosylated GSLs but increases intoxication, identifying fucosylated glycoproteins as functional receptors for CT. These findings provide insight into the molecular determinants regulating CT sensitivity of host cells.

Cholera is a diarrheal disease caused by the bacterium *Vibrio cholerae*[1]. Cholera toxin (CT) is an AB_5 protein toxin produced by *V. cholerae* that is the major virulence factor contributing to the disease. AB_5 family toxins have a single catalytic A subunit and five copies of the cell-surface-binding B subunit (CTB). The CT holotoxin binds to the surface of epithelial cells in the small intestine through the CTB and is subsequently internalized and retrograde transported through the Golgi to the endoplasmic reticulum (ER). The catalytic A subunit can then dissociate and translocate into the cytoplasm where it ADP-ribosylates Gαs, ultimately leading to ion dysregulation and massive release of fluid into the intestinal lumen[2]. Although diarrheal symptoms can be effectively treated with intravenous fluids or oral rehydration therapy, many fatalities still occur because of difficulties accessing treatment.

Studies in the 1970s identified a brain ganglioside, GM1, as a high affinity receptor for CT[3–8]. The interaction between CTB and the GM1 glycan has been structurally characterized[9,10] and the affinity depends mainly on the terminal Gal and Neu5Ac (sialic acid) residues, which are recognized in the canonical binding pocket[11]. Although GM1 is an effective receptor for CT in cell culture, disruption of GM1 biosynthesis in *B4galnt1*-knockout (KO) mice does not result in reduced CT intoxication relative to wild-type (WT) mice[12]. Furthermore, GM1 expression in human small intestine epithelial tissue is low[6,13]. In *V. cholerae* infection, additional GM1 may be produced through the action of *V. cholerae* neuraminidase[6,14]. However, *B4galnt1*-KO mouse intoxication occurred in the absence of *V. cholerae* neuraminidase, indicating that other receptor classes can function in CT intoxication.

[1]Department of Biochemistry, UT Southwestern Medical Center, Dallas, TX, USA. [2]Department of Microbiology and Immunology, Institute of Biomedicine, University of Gothenburg, Gothenburg, Sweden. [3]Complex Carbohydrate Research Center, The University of Georgia, Athens, GA, USA. [4]Department of Medical Biochemistry and Cell Biology, Institute of Biomedicine, University of Gothenburg, Gothenburg, Sweden. [5]McDermott Center for Human Growth and Development, UT Southwestern Medical Center, Dallas, TX, USA. [6]Department of Bioinformatics, UT Southwestern Medical Center, Dallas, TX, USA. e-mail: Jennifer.Kohler@UTSouthwestern.edu

https://doi.org/10.1038/s41589-024-01748-5

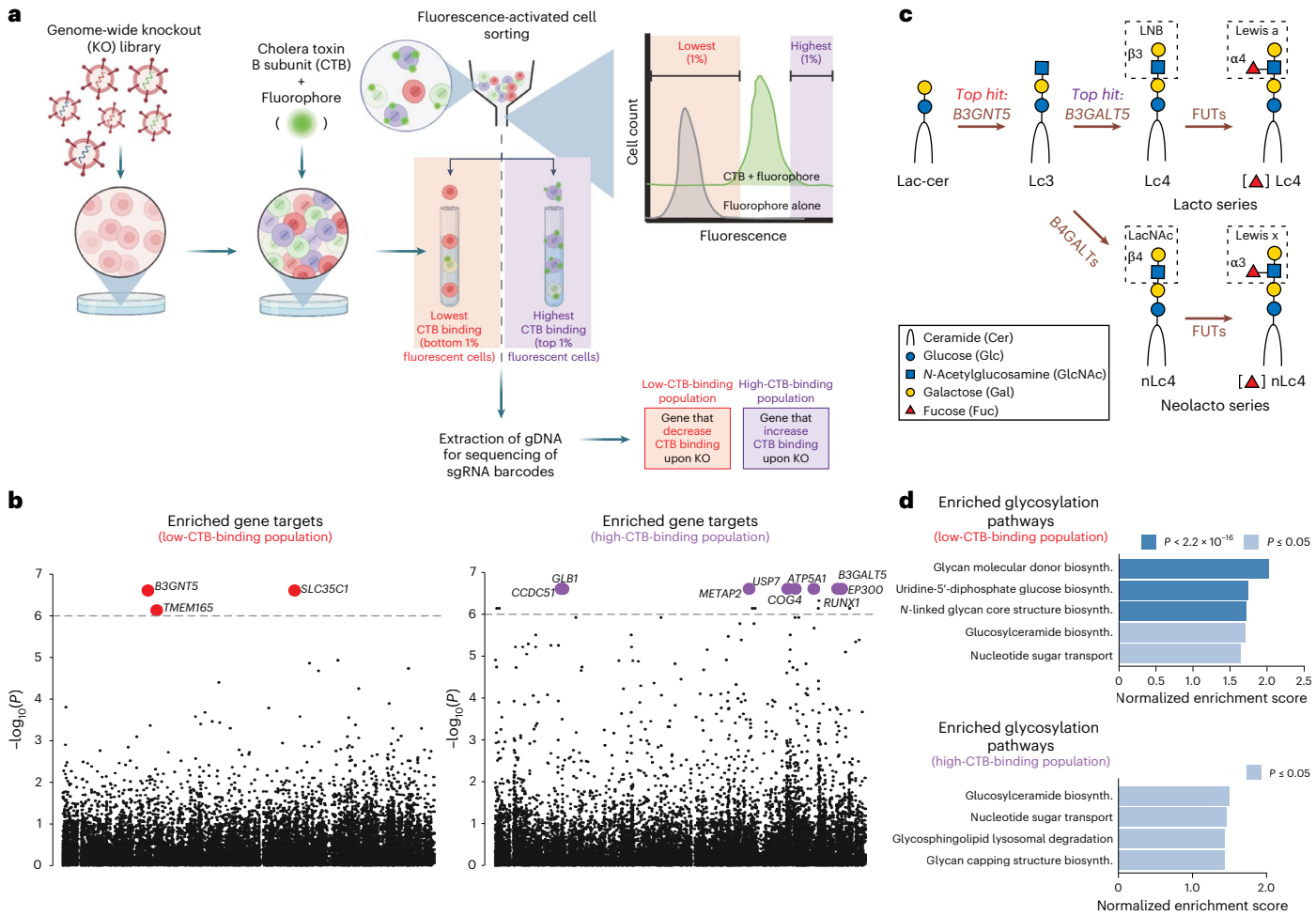

Fig. 1 | CRISPR screen for factors influencing CTB binding to Colo205 cells identifies GSL biosynthetic pathway genes. a, Schematic of genome-wide CRISPR KO screen for mediators of CTB binding to Colo205 intestinal epithelial cells using FACS to collect populations with low versus high CTB binding. **b**, Top sgRNA gene targets (unadjusted *P* value = 10^{-6}) enriched in the populations with low (left) and high (right) CTB binding relative to the unsorted input population of CRISPR KO library-expressing cells. The *y* axis shows unadjusted *P* values from a one-sided test for positive selection using the MAGeCK robust rank aggregation algorithm. **c**, Schematic of lacto and neolacto GSL biosynthetic pathway, which includes a top enriched sgRNA gene target of populations with both low and high CTB binding. **d**, GlycoEnzoOnto analysis results identify glycosylation pathways significantly enriched (Fisher's exact test) in the populations screened with low (top) and high (bottom) CTB binding. Dark-blue bars indicate an unadjusted *P* value < 2.2×10^{-16}. Light-blue bars indicate an unadjusted *P* value ≤ 0.05. The exact *P* values from most to least significant are as follows: 0.00235 and 0.0044 for glucosylceramide biosynthetic and nucleotide sugar transport pathways in the population with low CTB binding; 0.01218 and 0.0431 for the same pathways enriched in the population with high CTB binding; 0.04738 and 0.05 for the GSL lysosomal degradation and glycan capping structure biosynthetic pathways enriched in the population with high CTB binding. Created with BioRender.com. biosynth., biosynthetic pathway.

Fucosylated glycoconjugates have also been implicated as possible receptors for CT. Epidemiological studies have shown that the severity of cholera symptoms is increased in individuals with the O blood type[15–20]. The ABO blood types are defined by the expression of distinct, fucosylated antigens on the surface of the intestinal epithelium in addition to red blood cells. CT can directly bind ABO blood group antigens and the related Lewis antigens, which are also fucosylated[12,21–26]. Structural characterization of CTB revealed a second glycan-binding pocket distinct from the canonical GM1-binding pocket[21,27]. Fucosylated glycans are recognized in this noncanonical binding pocket. Although the affinity of CTB for fucosylated glycans is orders of magnitude lower than for GM1 (refs. 21,25), fucosylated glycoconjugates are abundant on the human small intestine epithelial cell surface[28]. Serendipitously, we found that CTB can bind to fucosylated glycoproteins from intestinal epithelial cell lines and that global reduction of fucosylation reduces CT binding and intoxication[29]. Nevertheless, the molecular details of fucosylated structures that regulate host cell intoxication remain incompletely defined.

Here, we report that two distinct classes of fucosylated glycoconjugates regulate CT activity in Colo205 cells. We find that β-1,3-*N*-acetylglucosaminyltransferase 5 (B3GNT5)-dependent, fucosylated glycosphingolipids (GSLs) act as decoy receptors for CT. Additionally, we observe that disruption of β-1,3-galactosyltransferase 5 (B3GALT5) activity results in increased production of fucosylated glycoproteins and promotes CT intoxication. Our data are consistent with a model in which the relative expression of fucosylated GSLs and fucosylated glycoproteins controls the extent of CT sensitivity in Colo205 cells.

Results

GSL biosynthetic genes affect CTB binding to Colo205 cells

We executed a genome-wide clustered regularly interspaced short palindromic repeats (CRISPR)–Cas9 KO screen to provide unbiased insight into glycoconjugates important for CTB binding to intestinal epithelial cells (Fig. 1a). Because our goal was to identify cell surface receptors for CTB, it was critical to avoid protease-based methods of

cell detachment. Therefore, we selected Colo205 cells (a colorectal cancer cell line that we used previously in studies of CT) as most suitable for our screening approach because of their sensitivity to EDTA as a dissociation reagent. We used fluorescence-activated cell sorting (FACS) to collect cells with altered CTB binding. We collected cells with the lowest 1% of fluorescence signal and cells with the highest 1% of fluorescence signal.

In the population with low CTB binding, three genes (*B3GNT5*, *SLC35C1* and *TMEM165*) were significantly enriched relative to the input control ($P < 10^{-6}$) (Fig. 1b, left). All three have clear links to glycosylation. This is consistent with CTB binding to cell surface glycoconjugates, which is well-documented[3–7,12,25,27,29–33]. *SLC35C1* is a gene that encodes the GDP-fucose transporter[34]. Work from our group and others has established that cell surface fucosylation has a role in CT binding and intoxication and CTB has been shown to bind directly to fucosylated glycans[12,21–23,25,27,29,31]. Mutations in enriched gene target *TMEM165* cause a human congenital disorder of glycosylation characterized by pleiotropic glycosylation abnormalities[35]. *B3GNT5* encodes an *N*-acetylglucosaminyltransferase that catalyzes addition of *N*-acetylglucosamine (GlcNAc) in a β1–3 linkage to galactose (Gal). The preferred substrate onto which B3GNT5 adds GlcNAc is the GSL lactosylceramide (Galβ1–4Glc-ceramide)[36]. The resulting GSL, Lc3 (GlcNAcβ1–3Galβ1–4Glc-ceramide) is the core structure from which all other lacto and neolacto series GSLs are generated.

In the population with high CTB binding, 17 genes were significantly enriched ($P < 10^{-6}$) (Fig. 1b, right). *B3GALT5*, which encodes a β1–3-galactosyltransferase that catalyzes the addition of Gal onto GlcNAc, was among the gene targets with highest enrichment in this population[37]. B3GALT5 is annotated to function in concert with B3GNT5 in the biosynthesis of lacto series GSLs (Fig. 1c)[38,39] and is highly expressed in Colo205 cells[40]. We also analyzed the CRISPR screening results using GlycoEnzoOnto ontology analysis for pathway identification (Fig. 1d)[41]. Multiple glycosylation pathways were significantly enriched ($P < 0.05$), including the nucleotide sugar transport and glucosylceramide biosynthesis pathways, which were enriched in both populations. The related pathways of GSL lysosomal degradation and glycolipid core biosynthesis were enriched in the populations with high and the low CTB binding, respectively.

Both the top hit from the population with high CTB binding (*B3GALT5*) and the top hit from the population with low CTB binding (*B3GNT5*) encode enzymes that have been shown to act on GSLs. Specifically, B3GNT5 catalyzes the formation of Lc3, which can serve as a substrate for B3GALT5 to produce lactotetraosylceramide (Lc4, Galβ1–3GlcNAcβ1–3Galβ1–4Glc-ceramide) (Fig. 1c). Alternately, Lc3 can be used as a substrate by B4GALTs to generate neolactotetraosylceramide (nLc4, Galβ1–4GlcNAcβ1–3Galβ1–4Glc-ceramide). To explore the role of GSLs, we used CRISPR–Cas9 to knock out *B3GALT5* and *B3GNT5* individually in Colo205 cells. We obtained two distinct monoclonal populations for each KO cell line (KO m1 and KO m2).

Increased CT binding and intoxication in *B3GALT5*-KO cells

Because B3GALT5 catalyzes Lc4 biosynthesis (Fig. 1c), we stained KO cells with antibodies specific for Lewis a (Le^a; Galβ1–3(Fucα1–4)GlcNAc-R), a fucosylated structure that can be displayed on lacto series GSLs. Le^a was completely lost from the surface of *B3GALT5*-KO cells and restored to control levels by stable overexpression (OE) of CRISPR–Cas9-resistant *B3GALT5* (*B3GALT5*-KO + OE) (Extended Data Fig. 1a). Conversely, *B3GALT5*-KO cells displayed increased expression of Lewis x (Le^x; Galβ1–4[Fucα1–3]GlcNAc-R), a fucosylated structure that can be displayed on neolacto series GSLs. Furthermore, *B3GALT5*-KO + OE cells showed reduced expression of Le^x as compared to control cells (Extended Data Fig. 1b). These results show that B3GALT5 controls expression of lacto-*N*-biose (LNB; Galβ1–3GlcNAc-R) glycans with inverse effects on expression of *N*-acetyllactosamine (LacNAc; Galβ1–4GlcNAc-R) glycans, consistent with prior work[38,39].

Both *B3GALT5*-KO m1 and *B3GALT5*-KO m2 cells exhibited increased CTB binding relative to a scramble single guide RNA (sgRNA)-expressing population, as predicted by the CRISPR screening results (Fig. 2a). The increase in CTB binding to *B3GALT5*-KO cells was apparent at a range of CTB concentrations (Extended Data Fig. 1c) and OE of B3GALT5 (*B3GALT5*-KO + OE) reverted CTB binding to below that of the scramble control cells (Fig. 2a). To see whether increased CTB binding to *B3GALT5*-KO cells had an impact on toxin function, we assayed toxin internalization in these cells. We treated cells with biotin–CTB complexed with streptavidin–saporin (CTB–saporin). Saporin is a cell-impermeable, ribosome-inactivating toxin[42,43]. Therefore, only active internalization of CTB–saporin can cause saporin-induced toxicity. CTB–saporin treatment caused a larger decrease in cell viability in both *B3GALT5*-KO m1 and *B3GALT5*-KO m2 cells as compared to control cells (Extended Data Fig. 1d). Because decreased cell viability is indicative of increased CTB–saporin internalization, this result is consistent with increased CTB binding to functional receptors on *B3GALT5*-KO cells. Cell viability was restored to control cell levels in *B3GALT5*-KO + OE cells. Importantly, treatment of all cell lines with unconjugated saporin resulted in minimal cell death, indicating that *B3GALT5*-KO cell susceptibility to CTB–saporin is not a result of non-specific toxin internalization (Extended Data Fig. 1e).

To further assess the impact of differential CTB binding and internalization on toxin function, we measured intoxication by CT. Consistent with the binding and internalization results, both *B3GALT5*-KO clones were more sensitive to CT, as evidenced by increased cyclic adenosine monophosphate (cAMP) accumulation relative to control cells (Fig. 2b). This increase was partially reversed in *B3GALT5*-KO + OE cells. To evaluate whether the observed cAMP accumulation was because of CT intoxication through the canonical pathway, we pretreated cells with brefeldin A (BFA), an antiviral agent that disrupts protein transport between the ER and Golgi, and then added CT. For all cell lines, CT-induced cAMP accumulation was reduced to basal levels (Extended Data Fig. 1f), indicating that a functional secretory pathway is required for CT-induced cAMP accumulation. Incubation of all cell lines with forskolin, a small-molecule activator of adenylyl cyclase, resulted in similar levels of cAMP accumulation (Extended Data Fig. 1g). This result demonstrated that the genetic KOs do not perturb cAMP signaling. We conclude that the observed differences in cAMP accumulation are because of differences in CT receptor expression on the cell surface.

Reduced binding but higher intoxication in *B3GNT5*-KO cells

In *B3GNT5*-KO cells, we observed a decrease in CTB binding, as predicted by the CRISPR screening results (Fig. 2c). The decrease in CTB binding to *B3GNT5*-KO cells was dose-dependent (Extended Data Fig. 2a). Stably overexpressing CRISPR–Cas9-resistant *B3GNT5* in *B3GNT5*-KO cells (*B3GNT5*-KO + OE cells) reverted CTB binding to above that of control cells (Fig. 2c). Because B3GNT5 is required for the biosynthesis of both lacto and neolacto series GSLs (Fig. 1c), we hypothesized that Le^a and Le^x expression would be reduced in *B3GNT5*-KO cells. Indeed, Le^x expression was significantly decreased in both *B3GNT5*-KO cell lines (Extended Data Fig. 2b). However, there was no significant difference in anti-Le^a staining among these cell lines (Extended Data Fig. 2c). Because *B3GNT5*-KO cells should not produce lacto series GSLs, this result suggested that most Le^a in Colo205 cells is displayed on glycoconjugates other than lacto series GSLs.

We assayed toxin internalization by treating cells with CTB–saporin. Although the differences were small, the effects on CTB internalization were consistent with the effects on CTB binding (Extended Data Fig. 2d,e). Next, we measured intoxication by CT. Both *B3GNT5*-KO cell lines were sensitized to CT relative to control cells (Fig. 2d and Extended Data Fig. 2f,g). This result was unexpected, as binding of CTB to the *B3GNT5*-KO cells was significantly decreased relative to control cells. Conversely, *B3GNT5*-KO + OE cells exhibited almost no cAMP accumulation upon incubation with CT, even though CTB binding

https://doi.org/10.1038/s41589-024-01748-5

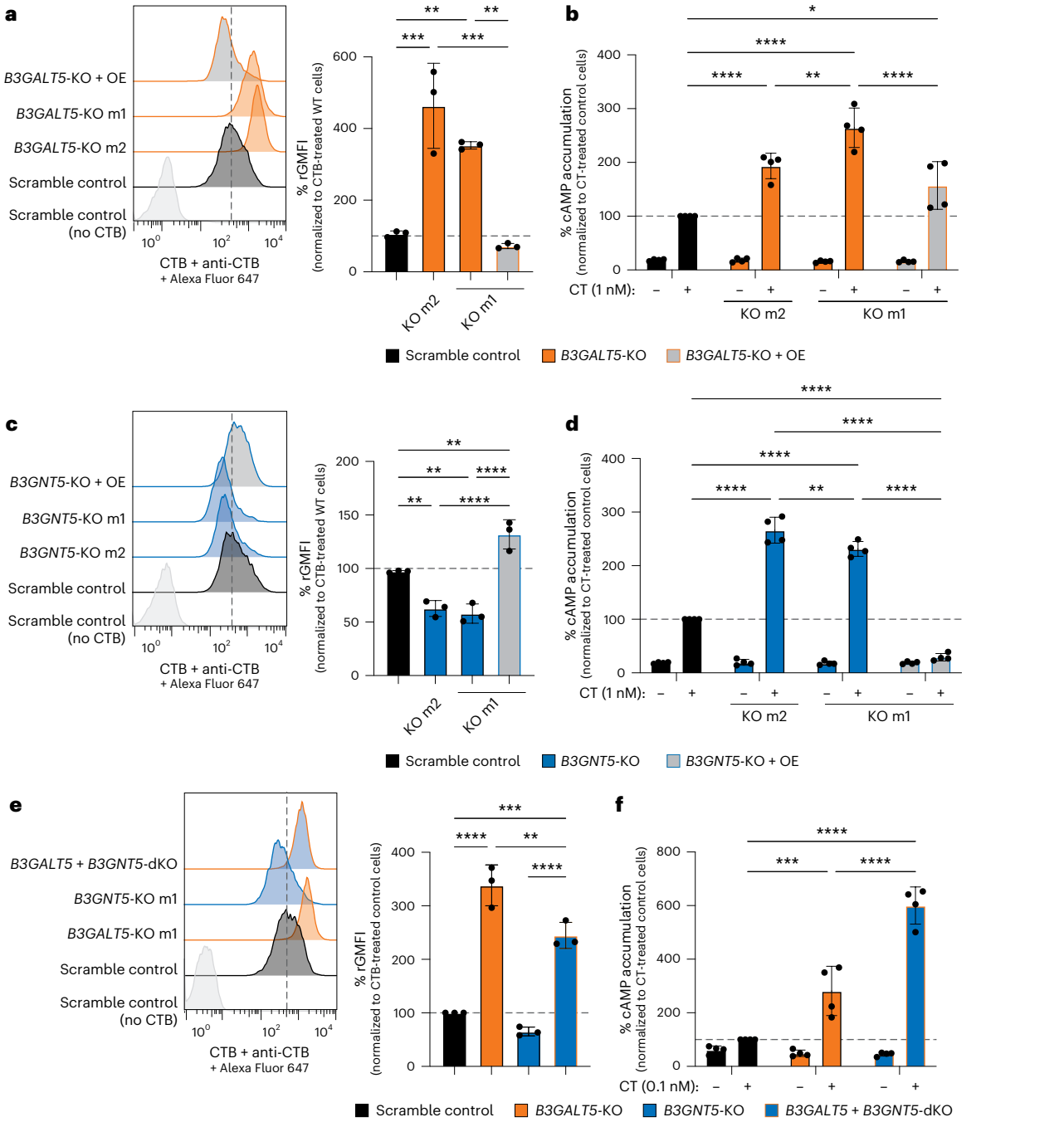

Fig. 2 | KO of *B3GALT5* and *B3GNT5* results in increased sensitivity to CT. **a**,**c**,**e**, Representative histograms from the flow cytometry analyses of cell surface binding of CTB (1 mg ml^{-1}) to control, KO, KO + OE and dKO cell lines. Bar graphs show quantification of geometric mean fluorescence index (gMFI) from three independent trials, normalized to the maximum APC signal in reference cells. Error bars indicate the mean ± s.d. Statistical analyses were performed by one-way analysis of variance (ANOVA) with Tukey correction. Adjusted *P* values are as follows: 0.0004 and 0.0043 for comparisons of control versus *B3GALT5*-KO m2 and m1 cells; 0.0004 and 0.0043 for *B3GALT5*-KO + OE cells versus *B3GALT5*-KO m2 and m1 cells (**a**); 0.0069 and 0.0031 for control versus *B3GNT5*-KO m2 and m1 cells; 0.0064 for control versus *B3GNT5*-KO + OE cells (**c**); 0.0003 and 0.0048 for comparisons of *B3GALT5* + *B3GNT5*-dKO versus control and *B3GALT5*-KO m1 cells, respectively (**e**). Vertical dashed lines in **a**, **c** and **e** indicate the gMFI of the CTB-treated scramble control population. Horizontal dashed lines in **a** and **c** indicate the normalized gMFI of the CTB-treated wild-type cell population. Horizontal dashed line in **e** indicates the normalized gMFI of the CTB-treated scramble control population. **b**,**d**,**f**, Control, KO, KO + OE and dKO cell lines were incubated for 1.5 h with cholera holotoxin. Accumulation of cAMP was measured using the cAMP-Glo Max assay. The total number of plated cells was measured using the Cell Titer-Glo 2.0 assay. Data shown are inverse cAMP values normalized first to the total number of cells plated for each cell line, then to the maximum signal in control cells. Each data point is a biological replicate consisting of three averaged technical replicates. Error bars indicate the mean ± s.d. of four biological replicates. Statistical analyses were performed by two-way ANOVA with Tukey correction. ****P (adjusted) < 0.0001. The remaining P values are as follows: 0.0229 for control versus *B3GALT5*-KO + OE cells and 0.0028 for *B3GALT5*-KO m2 versus *B3GALT5*-KO m1 cells (**b**); 0.0019 for *B3GNT5*-KO m2 versus *B3GNT5*-KO m1 cells (**d**); 0.0005 for control versus *B3GALT5*-KO m1 cells (**f**). Horizontal dashed lines in **b**, **d** and **f** indicate the normalized cAMP accumulation of CT-treated scramble control cells. Asterisks indicate significance as follows: *P < 0.05; **P < 0.01; ***P < 0.001.

and internalization were increased in these cells. Thus, the extent of intoxication by CT does not directly correlate with the amount of CTB binding, suggesting that not all CTB-binding molecules are functional receptors.

B3GALT5-KO effects are partially independent of *B3GNT5*

Because *B3GNT5*-KO cells exhibited increased intoxication despite decreased CTB binding, this implied the existence of decoy receptors whose expression is controlled by *B3GNT5*. In contrast, *B3GALT5*-KO cells exhibited both increased CTB binding and intoxication, which implied the existence of functional receptors. Thus, we hypothesized that more than one class of CTB-binding glycoconjugates exist in Colo205 cells. To directly test the role of lacto and neolacto series GSL biosynthesis in *B3GALT5*-KO cells, we used CRISPR–Cas9 to knock out *B3GNT5* in the *B3GALT5*-KO m1 cell line (*B3GALT5* + *B3GNT5*-double (d) KO). A monoclonal population of *B3GALT5* + *B3GNT5*-dKO cells exhibited decreased CTB binding relative to the parental *B3GALT5*-KO m1 cell line (Fig. 2e). However, binding was still significantly higher than in control and *B3GNT5*-KO m1 cells. Furthermore, Le^x expression in *B3GALT5* + *B3GNT5*-dKO cells was not significantly decreased relative to the parental *B3GALT5*-KO m1 population (Extended Data Fig. 3a). Together, these results confirmed that increased Le^x expression and increased CTB binding of *B3GALT5*-KO cells were independent of the lacto and neolacto series GSL biosynthetic pathway.

We also assayed toxin internalization and intoxication in the *B3GALT5* + *B3GNT5*-dKO cells. The *B3GALT5* + *B3GNT5*-dKO and *B3GALT5*-KO cells were indistinguishable in the internalization analysis (Extended Data Fig. 3b,c) but differences were observed in the intoxication assay. Strikingly, *B3GALT5* + *B3GNT5*-dKO cells exhibited increased cAMP signal upon treatment with CT, even relative to the sensitized *B3GALT5*-KO m1 parental cell line (Fig. 2f and Extended Data Fig. 3d,e). Although the *B3GALT5*-KO and *B3GALT5* + *B3GNT5*-dKO cells did not exhibit measurable differences in the internalization assay, these intoxication data support our proposal that *B3GALT5*-KO cells produce functional receptors for CT while *B3GNT5*-KO cells lose production of decoy receptors for CT.

GSLs act as decoy receptors for CT

Because loss of B3GNT5 activity sensitized cells to CT, we considered the possibility that *B3GNT5*-KO might shunt precursor GSLs to the biosynthesis of other GSLs such as GM1. We, therefore, assessed the GSL composition of *B3GNT5*-KO, *B3GALT5*-KO and control cells by nanoelectrospray ionization tandem mass spectrometry (nESI-MS/MS) (Fig. 3a and Extended Data Fig. 4a–c). While GM1 was not detected in any of the cell lines, control cells expressed extended, fucosylated GSLs, which were identified by accurate mass and MS/MS fragmentation analysis (Extended Data Fig. 4d).

Because GM1 was not detected in *B3GALT5*-KO cells, we hypothesized that these cells might display increased CTB binding because of altered protein glycosylation. To test this, we performed lectin blot analysis of lysates, probing with biotin–CTB. We observed increased CTB recognition of multiple species with high (>50 kDa) and low (<37 kDa) apparent molecular weight (MW) in *B3GALT5*-KO m1 and m2 cell lysates as compared to control cell lysates (Fig. 3b). These bands were not observed in *B3GALT5*-KO + OE rescue cell lysates or in those of *B3GNT5*-KO cell lines. Only one band (~10 kDa apparent MW) was recognized by CTB in lysates of *B3GNT5*-KO + OE cells. Because these cells were significantly protected against CT intoxication while *B3GNT5*-KO cells were sensitized to intoxication, we hypothesized that this band might consist of decoy receptors for CT synthesized by B3GNT5. The low apparent MW (~10 kDa) of the band indicated that the putative decoy receptor might be a GSL. We therefore treated lysates with proteinase K or endoglycoceramidase (EGCase) before lectin blot analysis. Proteinase K is a nonspecific protease that digests all proteins, while EGCase is an enzyme that cleaves the glycan headgroup from GSLs. We also included *B3GALT5*-KO cells in this analysis because additional species with a low apparent MW (~20 kDa) were detected in these lysates. Indeed, both bands with low apparent MW (10 and 20 kDa) recognized by CTB were sensitive to EGCase but not to proteinase K, confirming that these are indeed GSLs (Fig. 3c). To validate our method, we made use of GM1, a GSL that is also a known receptor of CTB[3–7,30]. Purified GM1 was readily detected by CTB lectin blot and treatment with EGCase completely abrogated detection (Extended Data Fig. 5a). Importantly, GM1 migrated at a lower apparent MW than the species detected in Colo205 cell lysates.

To assess whether GSLs function as decoy receptors for CT, we treated cells with P4, an inhibitor of GSL biosynthesis[44]. We performed lectin blot analysis to ensure the specific GSLs of interest were decreased. As expected, cells treated with P4 displayed reduced expression of the GSLs with low MW (~10 and ~20 kDa) (Fig. 3d and Extended Data Fig. 5b). We then measured the intoxication of P4-treated cells by measuring cAMP accumulation. P4 treatment of *B3GALT5*-KO cells did not have a significant impact on intoxication (Extended Data Fig. 5c–e). However, *B3GNT5*-KO + OE cells were no longer protected against CT, as seen by cAMP accumulation returning to levels similar to those of control cells (Fig. 3e and Extended Data Fig. 5f,g). This result is consistent with the hypothesis that the ~10-kDa GSL species present in *B3GNT5*-KO + OE cells is a decoy receptor.

We used MS to gain insight into the molecular identity of this putative decoy receptor. Analysis of intact GSLs from *B3GNT5*-KO + OE cells by nESI-MS/MS was not sufficiently sensitive; thus, glycans were released with EGCase, labeled with procainamide and analyzed by MS with hydrophilic interaction liquid chromatography and fluorescence (HILIC-FL) separation. This analysis identified several neutral glycans present in *B3GNT5*-KO + OE cells that were absent from *B3GALT5*-KO cells (Extended Data Fig. 6a). On the basis of this result, we isolated neutral GSLs from the *B3GNT5*-KO + OE cells. The neutral GSL mixture was treated with EGCase, and then liquid chromatography (LC)–ESI-MS was used to characterize the released oligosaccharides (Extended Data Fig. 6b). A variety of fucosylated GSLs were detected including large structures with up to three fucose residues (Extended Data Fig. 6c). To test whether these GSLs could function as decoy receptors, we added them to *B3GALT5* + *B3GNT5*-dKO cells and measured the impact on CT-induced cAMP accumulation. The cells were protected from CT-induced cAMP accumulation in a dose-dependent manner (Fig. 3f and Extended Data Fig. 6d,e), consistent with our proposal that these GSLs are decoy receptors. To assess whether our method allowed for GSL incorporation in the plasma membrane, we added GM1 to the *B3GALT5* + *B3GNT5*-dKO cells and showed that the cells became more susceptible to CT-induced cAMP accumulation. As an additional control, cells were treated with a commercial mixture of neutral, non-fucosylated glycolipids, resulting in no impact on CT-induced cAMP accumulation. Of note, the commercial neutral glycolipid mixture included Gb3 and Gb4, which were detected in the MS analysis of GSLs from *B3GNT5*-KO + OE cells. Thus, these results implicate fucosylated GSLs as decoy receptors for CT.

Fucosylation is required for intoxication of *B3GALT5*-KO cells

Because *B3GALT5* + *B3GNT5*-dKO cells were more sensitized to CT than other cell lines (Fig. 2f), we hypothesized that they produce functional CT receptors. Lectin blot analysis revealed that *B3GALT5*-KO results in increased production of glycoproteins that are recognized by CTB (Fig. 3b). We therefore used MS to assess the *N*-linked and *O*-linked glycan composition on proteins isolated in triplicate from *B3GALT5*-KO or control cells by LC–MS/MS. Both *N*-linked and *O*-linked glycans extracted from *B3GALT5*-KO cells were larger than those from control cells (Fig. 4 and Extended Data Figs. 7a and 8a). Glycans from *B3GALT5*-KO cells were also more highly fucosylated. *N*-linked glycan structures with multiple fucose residues were detected (Extended Data Fig. 7b) and *N*-linked glycans with two or more fucose residues

https://doi.org/10.1038/s41589-024-01748-5

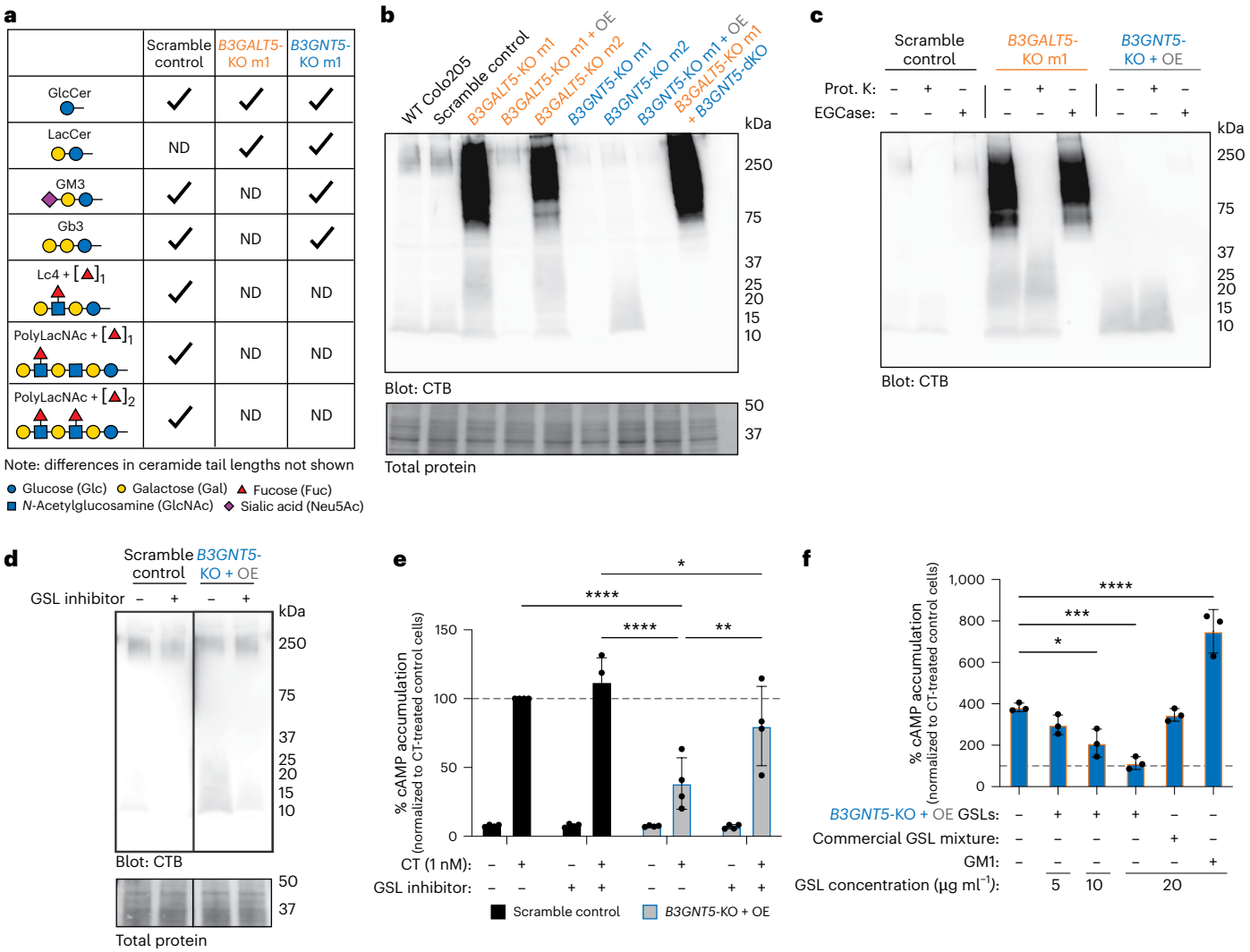

Fig. 3 | GSLs are decoy receptors for CT. a, Table of glycan headgroups detected by MS analysis of intact glycolipids extracted from control, *B3GALT5*-KO m1 and *B3GNT5*-KO m1 cells. 'ND' indicates that the glycan headgroup was not detected in the corresponding cell line. **b**, Lectin blot with CTB–biotin of lysates from control, *B3GALT5*-KO m1, *B3GNT5*-KO m1, respective KO + OE and *B3GALT5* + *B3GNT5*-dKO cells. Data shown are a single representative trial of three independent biological replicates. **c**, Lectin blot with CTB–biotin of control, *B3GALT5*-KO m1 and *B3GNT5*-KO + OE cell lysates treated for 16 h with proteinase K, EGCase or a vehicle control. Data shown are a single representative trial of three independent biological replicates. **d**,**e**, Control and *B3GNT5*-KO + OE cells were treated with P4 inhibitor of GSL biosynthesis for 72 h. Treated cells were lysed and subjected to lectin blot analysis with CTB–biotin (**d**) or incubated for 1.5 h with CT (1 nM; **e**) for analysis of cAMP accumulation. The lectin blot shown is a single representative trial of two independent biological replicates and is spliced from a single membrane, as indicated by the vertical line. **f**, *B3GALT5* + *B3GNT5*-dKO cells were incubated with neutral GSLs extracted from *B3GNT5*-KO + OE cells, a commercial mixture of neutral GSLs, or purified GM1 and then treated with CT (0.25 nM) for analysis of cAMP accumulation. cAMP accumulation data are inverse luminescence values normalized to the total number of cells then to the maximum signal in control cells. Each data point is a biological replicate consisting of three (**e**) or 2 (**f**) averaged technical replicates. Error bars indicate the mean ± s.d. of four (**e**) or three (**f**) biological replicates. Statistical analysis was performed by two-way (**e**) or one-way (**f**) ANOVA with Tukey correction. ****P (adjusted) < 0.0001. The remaining P values are as follows: 0.0498 and 0.0049 for inhibitor-treated *B3GNT5*-KO + OE cells versus inhibitor-treated control and vehicle-treated *B3GNT5*-KO + OE cells (**e**); 0.0198 and 0.0004 for solvent-treated *B3GALT5* + *B3GNT5*-dKO cells versus 10 and 20 mg ml^{-1} *B3GNT5*-KO + OE GSL-treated *B3GALT5* + *B3GNT5*-dKO cells. Horizontal dashed lines in **e** and **f** indicate the normalized cAMP accumulation of CT-treated scramble control cells. Asterisks indicate significance as follows: *P < 0.05; **P < 0.01; ***P < 0.001.

were enriched in *B3GALT5*-KO cells (Extended Data Fig. 7c). Even more dramatic differences were detected for *O*-GalNAc glycans. The monofucosylated, singly extended core 2 *O*-glycan (Galβ(1–3/4)(Fucα1–2/3/4)GlcNAcβ(1–6)(Galβ(1–3))GalNAcαSer/Thr) was the only fucosylated *O*-glycan detected in control cells whereas in *B3GALT5*-KO cells, an abundance of large, multiply extended core 2 glycans displaying multiple fucose residues were detected (Fig. 4a and Extended Data Fig. 8a–c). Thus, *B3GALT5*-KO cells are enriched in the expression of fucosylated glycoproteins.

We were surprised to observe the dramatic difference in *O*-linked glycan structure in control versus *B3GALT5*-KO cells, including the striking observation that the control cells have high levels of the tumor-associated Tn and T antigens. This result suggests that the high level of B3GALT5 in Colo205 cells[40] shapes the glycome in a way that protects cells from CT. To investigate whether the catalytic activity of B3GALT5 was required for protection of cells from CT, we expressed inactive B3GALT5 in the *B3GALT5*-KO cells (*B3GALT5*-KO + mut OE). While WT B3GALT5 rescued CTB binding and CT intoxication, expression of inactive B3GALT5 had no effect on CTB binding as measured by flow cytometry and no significant effect on CT-induced cAMP accumulation (Fig. 4b,c and Extended Data Fig. 8d,e). These results indicate that the catalytic activity of B3GALT5 is required for its protective

https://doi.org/10.1038/s41589-024-01748-5

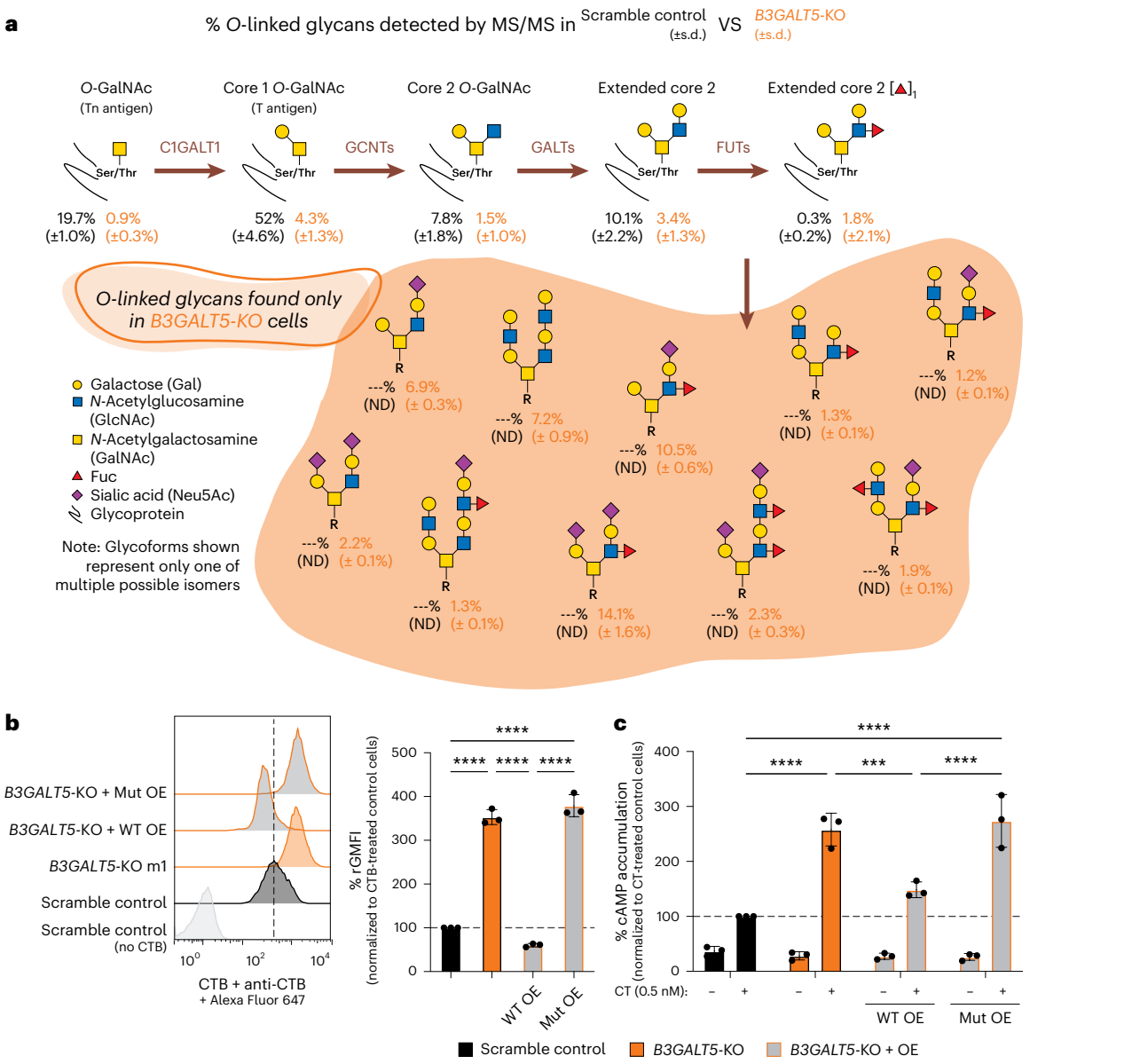

Fig. 4 | *B3GALT5*-KO cells exhibit increased fucosylation on *O*-linked glycoproteins. a, Schematic of *O*-linked glycan biosynthesis. Relative enrichment is included below each structure as detected by LC–MS/MS of glycans from control and *B3GALT5*-KO m1 cells. 'ND' indicates glycans that were not detected in corresponding cell line. Glycans that were detected in *B3GALT5*-KO m1 cells but not in control cells are highlighted by an orange background. **b**,**c**, *B3GALT5*-KO m1 cells were rescued with either WT or catalytically dead (mut) *B3GALT5*-OE. Rescued cells were analyzed alongside control and parental *B3GALT5*-KO m1 cells for CTB (1 mg ml^{-1}) binding by flow cytometry (**b**) and cAMP accumulation upon CT (0.5 nM) intoxication (**c**). Error bars indicate the mean ± s.d. Statistical analyses were performed by one-way (**b**) or two-way (**c**) ANOVA with Tukey correction. ****P (adjusted) < 0.0001. The adjusted P value for *B3GALT5*-KO m1 cells versus *B3GALT5*-KO + WT OE cells is 0.0002. Vertical and horizontal dashed lines in **b** indicate the gMFI and the normalized gMFI of the CTB-treated scramble control population, respectively. Horizontal dashed line in **c** indicates the normalized cAMP accumulation of CT-treated scramble control cells. Asterisks indicate significance as follows: ***P < 0.001.

effects on CTB binding and CT intoxication but the exact mechanism remains undefined.

To assess the role of fucosylation, we used CTB mutants that have a point substitution in either of the glycan-binding pockets (Fig. 5a)[45]. The W88K point substitution in the canonical binding pocket abrogates CTB binding to the GM1 glycan but binding to fucosylated glycans is unaffected. Conversely, the H18L point substitution in the noncanonical binding pocket disrupts CTB binding to fucosylated glycans but binding to GM1 is unaffected. We analyzed binding of biotinylated CTB mutants alongside WT CTB to control and *B3GALT5*-KO cells. In both *B3GALT5*-KO and control cells, the W88K CTB mutant retained almost all binding, whereas the H18L mutant exhibited significantly decreased binding relative to WT CTB (Fig. 5b). CTB blot analysis confirmed that binding to both glycoproteins and glycolipids is dependent on the noncanonical pocket (Fig. 5c), whereas binding to GM1 depends on the canonical pocket (Extended Data Fig. 9a). To check the functional importance, we used the CTB–saporin internalization assay. Treatment of both control and *B3GALT5*-KO cells with W88K CTB–saporin resulted in little change in cell survival relative to WT CTB–saporin treatment (Fig. 5d). Treatment of both control and *B3GALT5*-KO cells with H18L CTB–saporin resulted in a complete protection from saporin-induced cell death. Together, these data demonstrate that the noncanonical binding pocket is required for CTB binding to and internalization in both *B3GALT5*-KO and control cells but the canonical binding pocket is not.

To further assess the functional importance of fucosylation, we used CRISPR–Cas9 to knock out the gene encoding the GDP-fucose

https://doi.org/10.1038/s41589-024-01748-5

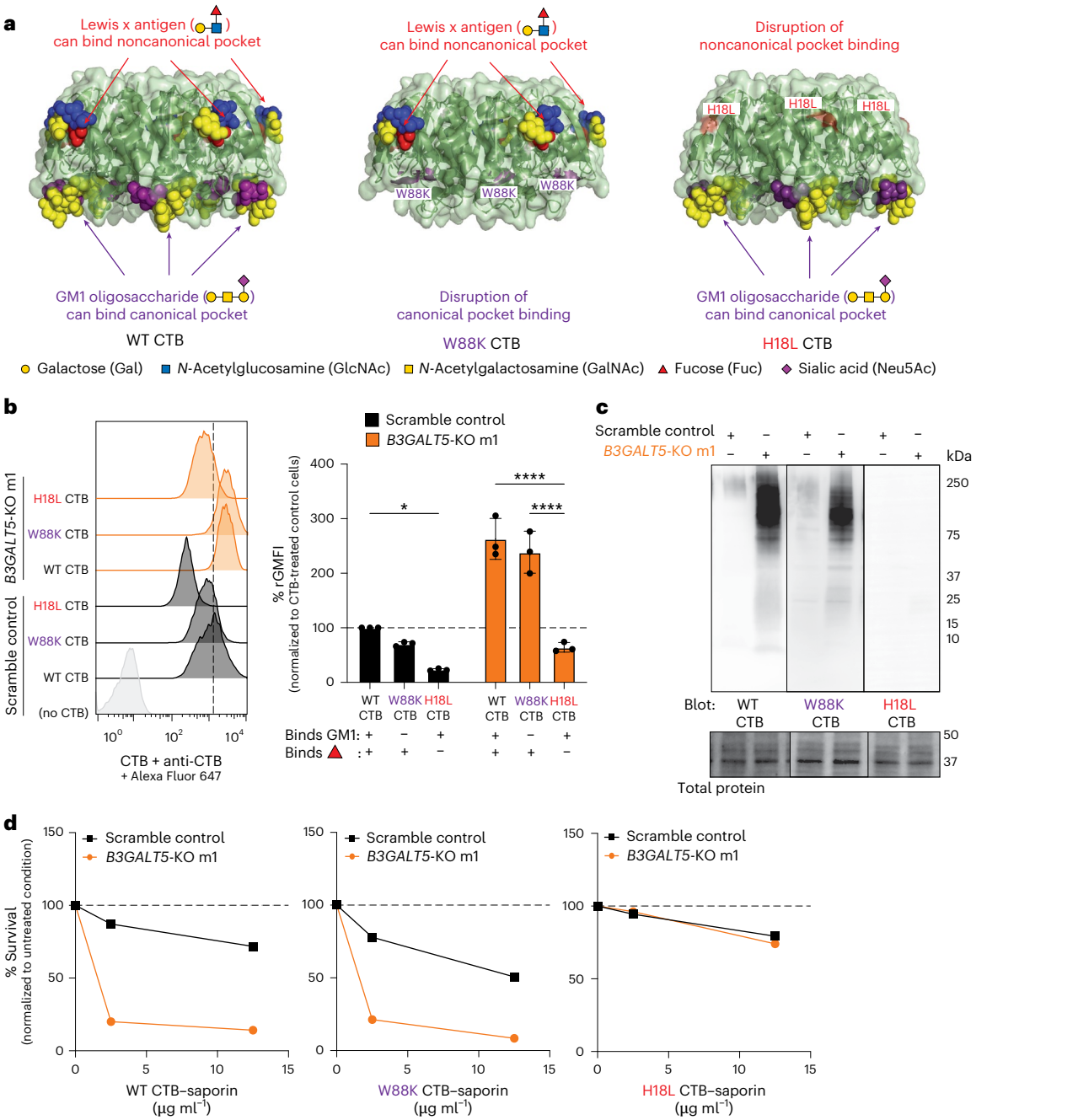

Fig. 5 | CTB binding to Colo205 cells depends on the noncanonical glycan-binding pocket. a, Structure of CTB pentamer illustrating the canonical and noncanonical binding pockets. Protein and GM1 coordinates[10] and Le^x coordinates[27] were taken from previously determined CTB structures and aligned using PyMOL. The locations of the W88K point substitution in the canonical binding pocket and the H18L point substitution in the noncanonical binding pocket are highlighted. **b**, Representative flow cytometry histograms of control and *B3GALT5*-KO m1 cells incubated with WT CTB, W88K CTB or H18L CTB (1 mg ml^{-1}). Data shown are a single representative trial from three independent experiments. Bar graphs show the quantification of gMFI from the three independent trials normalized to the maximum signal in control cells. Error bars indicate the mean ± s.d. Statistical analyses were performed by two-way ANOVA with Tukey correction. ****P (adjusted) < 0.0001. The adjusted P value for control cells treated with WT versus H18L CTB is 0.0114. Vertical and horizontal dashed lines in **b** indicate the gMFI and the normalized gMFI of the CTB-treated scramble control population, respectively. Asterisks indicate significance as follows: *P < 0.05. **c**, Lysates from *B3GALT5*-KO m1 and control cells were analyzed by lectin blot, probing with either WT or mutant CTB–biotin. Blots shown are from three distinct membranes (separated by vertical lines) processed simultaneously. Each blot is a single representative trial of three independent biological replicates. **d**, *B3GALT5*-KO m1 and control cells were incubated for 72 h with increasing concentrations of WT, W88K or H18L CTB–saporin. Cell survival was measured using the Cell Titer-Glo 2.0 assay. Data shown are luminescence values normalized to the maximum signal for each cell type. Each data point is the average of two biological replicates, each consisting of three averaged technical replicates. Horizontal dashed lines in **d** indicate normalized survival with no CTB–saporin.

transporter *SLC35C1* in WT and *B3GALT5*-KO cells. We confirmed that Le^x and other fucosylated glycans were absent from these cells (Extended Data Fig. 9b–d). We observed dramatically reduced CTB binding to both *SLC35C1*-KO and *B3GALT5* + *SLC35C1*-dKO cells relative to *B3GALT5*-KO cells (Fig. 6a,b). To identify fucosylated proteins recognized by CTB, we conducted affinity purification from lysates from the highly sensitized *B3GALT5* + *B3GNT5*-dKO cells and the protected *B3GALT5* + *SLC35C1*-dKO cells using biotinylated CTB (Extended Data

https://doi.org/10.1038/s41589-024-01748-5

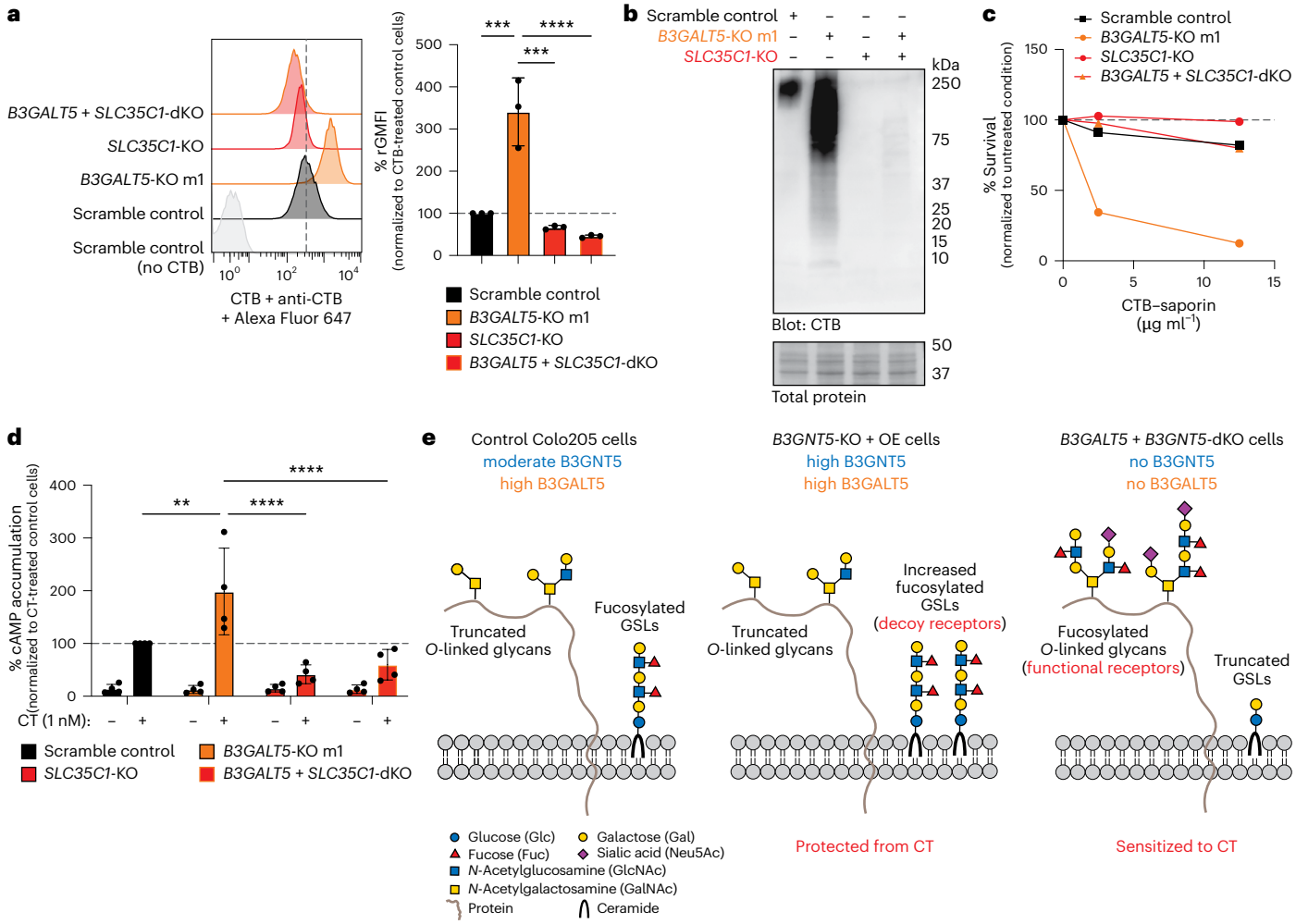

Fig. 6 | Fucosylated glycoproteins and fucosylated glycolipids have opposing roles in CT intoxication. a, Left: representative histograms from the flow cytometry analyses of CTB (1 mg ml^{-1}) binding to surfaces of control, *B3GALT5*-KO m1, *SLC35C1*-KO and *B3GALT5* + *SLC35C1*-dKO cells. Data shown are a single representative trial from three independent experiments. Right: quantification of gMFIs from the three independent trials are normalized to the maximum signal in control cells. Error bars indicate the mean ± s.d. Vertical and horizontal dashed lines in **a** indicate the gMFI and the normalized gMFI of the CTB-treated scramble control population, respectively. Asterisks indicate significance as follows: ***$P < 0.001$. **b**, Lysates from control, *B3GALT5*-KO, *SLC35C1*-KO and *B3GALT5* + *SLC35C1*-dKO cells were analyzed by lectin blot, probing with CTB–biotin. Data shown are a single representative trial of three independent biological replicates. **c**, Control, *B3GALT5*-KO m1, *SLC35C1*-KO and *B3GALT5* + *SLC35C1*-dKO cells were incubated for 72 h with increasing concentrations of CTB–saporin. Cell survival upon internalization of CTB–saporin was measured. Data shown are luminescence values normalized to the signal from the untreated condition for each cell type. Data points are the average of $n = 2$ biological replicates each consisting of three averaged technical replicates. **d**, Control, *B3GALT5*-KO m1, *SLC35C1*-KO and *B3GALT5* + *SLC35C1*-dKO cells were incubated for 1.5 h with CT (1 nM), after which accumulation of cAMP was measured. Data shown are inverse luminescence values normalized to the total number of cells and then to the maximum signal in control cells. Each data point is a biological replicate consisting of three averaged technical replicates. Error bars indicate the mean ± s.d. of four biological replicates. Statistical analyses were performed by one-way ANOVA (**a**) and two-way ANOVA (**d**) with Tukey correction. ****P (adjusted) < 0.0001. The adjusted P values for *B3GALT5*-KO m1 versus control and *SLC35C1*-KO cells (**a**) are 0.0004 and 0.0002, respectively. The adjusted P value for *B3GALT5*-KO m1 versus control cells (**d**) is 0.0043. Horizontal dashed line in **d** indicates the normalized cAMP accumulation of CT-treated scramble control cells. Asterisks indicate significance as follows: **$P < 0.01$. **e**, Model depicting how B3GNT5 and B3GALT5 regulate the production of CT receptors. Representative glycan structures presented in this model are postulated on the basis of *O*-linked glycomic analysis of control and *B3GALT5*-KO Colo205 cells and glycolipidomic analysis of control, *B3GALT5*-KO and *B3GNT5*-KO Colo205 cells.

Fig. 10a,b). We selected two top hits, mucin 1 (MUC1) and flotillin 1 (FLOT1), for validation. While the same amounts of MUC1 and FLOT1 were present in both cell lines, more of both MUC1 and FLOT1 were purified from the *B3GALT5* + *B3GNT5*-dKO cells as compared to the *B3GALT5* + *SLC35C1*-dKO cells (Extended Data Fig. 10c). These results show that glycan structure impacts CTB interactions with plasma membrane glycoproteins and that CTB associates with more than one plasma membrane glycoprotein. We also observed that both *SLC35C1*-KO and *B3GALT5* + *SLC35C1*-dKO cells were completely protected from CTB–saporin-induced cell death (Fig. 6c and Extended Data Fig. 9e). Lastly, to test whether the loss of CTB binding in *SLC35C1*-KO cells impacted intoxication, we treated cells with unlabeled CT and measured cAMP accumulation. We found that the loss of *SLC35C1* was protective against cholera intoxication even in the background of the sensitized *B3GALT5*-KO cells (Fig. 6d and Extended Data Fig. 9f,g). Together, these results show that sensitization to CT in *B3GALT5*-KO cells is dependent on fucosylation.

Discussion

Here, we report that the glycosyltransferases B3GALT5 and B3GNT5 are regulators of CT binding and intoxication of Colo205 cells (Fig. 6e). These enzymes control the expression of fucosylated

glycoconjugates that are recognized by CTB. B3GNT5 controls the expression of fucosylated GSLs that act as decoy receptors. Addition of these fucosylated GSLs to cells protects them from CT intoxication. This contrasts with the sensitization to CT that occurs with the addition of GM1, as seen in our control experiment and classical studies of CT intoxication[3,6,46]. Genetic disruption of *B3GALT5* allows for the biosynthesis of fucosylated *O*-linked glycoproteins that bind CTB and promote intoxication. The interplay of B3GALT5 and B3GNT5 activity determines which fucosylated structures are produced and whether they are displayed on glycoproteins versus GSLs.

Pioneering CRISPR screens using CT as a model system also found activation of *B3GNT5* to be protective against intoxication[47]. This consistency is especially striking because the lymphoblast cell line used expresses detectable GM1 (ref. 48). Indeed, the top glycosylation genes identified in these earlier screens were involved in ganglioside biosynthesis. These genes were not enriched in our screen, suggesting that GM1 does not contribute significantly to CTB binding to Colo205 cells. Our data, however, do not exclude a role for GM1 or other nonfucosylated receptors in CT intoxication. For instance, we observed intoxication of *SLC35C1*-KO cells albeit at low levels, suggesting that other nonfucosylated receptors for CT might exist. GM1 was not detected in MS analysis of GSLs from Colo205 cells, which is consistent with minimal GM1 expression in normal human intestinal epithelial tissue[6,13]. Nevertheless, because of the high affinity of the interaction between GM1 and CTB, only small amounts may be necessary. In addition, highly abundant receptors such as fucosylated glycoproteins could act in concert with low-abundance receptors such as GM1 to drive intoxication[27]. Indeed, even in the presence of detectable GM1, fucosylated glycoconjugates can affect CT activity[31,47].

Our data demonstrate that fucosylated GSLs protect cells from CT but we do not yet understand the mechanism of protection. One possibility is that fucosylated GSLs sequester CT from fucosylated glycoproteins that actively facilitate internalization. Such sequestration could occur on the cell surface or, alternately, CTB-binding fucosylated GSLs could be shed from the cell surface. Fucosylated GSLs could also control CT trafficking. In the case of GM1, changes to the ceramide impact nanodomain assembly and endocytic trafficking[49,50]; it remains to be investigated whether similar observations hold true for fucosylated GSLs. Regarding fucosylated glycoproteins that promote intoxication, proteomic analysis of CTB-binding glycoproteins yielded a number of candidate receptors; future work will explore which of these interact directly with CTB and contribute to the internalization mechanism. FLOT1 is an intriguing candidate because of its role in clathrin-independent endocytosis, a pathway that CT uses for cell entry[51]. *B3GALT5*-KO cells exhibit increased fucosylation of both *N*-linked and *O*-linked glycans; our current data do not assess the relative importance of these classes of glycans in CT intoxication. Furthermore, KO of *B3GALT5* results in a dramatic shift in *O*-glycan composition from mainly tumor-associated truncated *O*-glycans to diversely complex, fucosylated core 2 *O*-glycans. This change is associated with increased sensitivity to CT; however, normal human intestinal epithelia also display abundant core 3 extended *O*-glycan structures not examined here[52,53]. Indeed, one limitation of the current work is that it was performed in a colorectal cancer cell line. A study performed using human enteroids derived from jejunal biopsies also implicated fucose as having a dual role in contributing to both functional and decoy receptors[45]. In the enteroid study, which relied on use of small-molecule inhibitors of glycosylation, the apparent contributions of glycolipids and glycoproteins were the reverse of what we propose here. Together, these two studies firmly establish roles for fucosylated glycoconjugates in CT intoxication and protection but additional work is required to fully reconcile the results and define molecular features that distinguish functional and decoy receptors.

Intestinal epithelial fucosylation has implications in human health and disease[54,55]. Commensal bacteria induce fucosylation of intestinal epithelia, supporting host–microbe symbiosis in the face of pathogenic challenge[56–59]. Pathogens such as *Campylobacter jejuni* and *Salmonella* Typhimurium use host fucose as an energy source[60–62]. These pathogens and others are able to recognize and discriminate among blood group and other fucosylated glycans present in the intestine[63–80]. The data presented here further highlight the importance of understanding the regulation and composition of fucosylated structures in the human gut.

Online content

Any methods, additional references, Nature Portfolio reporting summaries, source data, extended data, supplementary information, acknowledgements, peer review information; details of author contributions and competing interests; and statements of data and code availability are available at https://doi.org/10.1038/s41589-024-01748-5.

References

1. Grant, T. A., Balasubramanian, D. & Almagro-Moreno, S. JMM profile: *Vibrio cholerae*: an opportunist of human crises. *J. Med. Microbiol.* **70**, 001423 (2021).
2. White, C., Bader, C. & Teter, K. The manipulation of cell signaling and host cell biology by cholera toxin. *Cell Signal.* **100**, 110489 (2022).
3. Cuatrecasas, P. Gangliosides and membrane receptors for cholera toxin. *Biochemistry* **12**, 3558–3566 (1973).
4. Cuatrecasas, P., Parikh, I. & Hollenberg, M. D. Affinity chromatography and structural analysis of *Vibrio cholerae* enterotoxin–ganglioside agarose and the biological effects of ganglioside-containing soluble polymers. *Biochemistry* **12**, 4253–4264 (1973).
5. Heyningen, S. V. Cholera toxin: interaction of subunits with ganglioside GM1. *Science* **183**, 656–657 (1974).
6. Holmgren, J., Lonnroth, I., Mansson, J. & Svennerholm, L. Interaction of cholera toxin and membrane GM1 ganglioside of small intestine. *Proc. Natl Acad. Sci. USA* **72**, 2520–2524 (1975).
7. King, C. A. & Van Heyningen, W. E. Deactivation of cholera toxin by a sialidase-resistant monosialosylganglioside. *J. Infect. Dis.* **127**, 639–647 (1973).
8. Holmgren, J., Lönnroth, I. & Svennerholm, L. Tissue receptor for cholera exotoxin: postulated structure from studies with GM1 ganglioside and related glycolipids. *Infect. Immun.* **8**, 208–214 (1973).
9. Merritt, E. A. et al. Structural studies of receptor binding by cholera toxin mutants. *Protein Sci.* **6**, 1516–1528 (1997).
10. Merritt, E. A. et al. Crystal structure of cholera toxin B-pentamer bound to receptor GM1 pentasaccharide. *Protein Sci.* **3**, 166–175 (1994).
11. Turnbull, W. B., Precious, B. L. & Homans, S. W. Dissecting the cholera toxin–ganglioside GM1 interaction by isothermal titration calorimetry. *J. Am. Chem. Soc.* **126**, 1047–1054 (2004).
12. Cervin, J. et al. GM1 ganglioside-independent intoxication by cholera toxin. *PLoS Pathog.* **14**, e1006862 (2018).
13. Breimer, M. E., Hansson, G. C., Karlsson, K. A., Larson, G. & Leffler, H. Glycosphingolipid composition of epithelial cells isolated along the villus axis of small intestine of a single human individual. *Glycobiology* **22**, 1721–1730 (2012).
14. Alisson-Silva, F. et al. Human evolutionary loss of epithelial Neu5Gc expression and species-specific susceptibility to cholera. *PLoS Pathog.* **14**, e1007133 (2018).
15. Glass, R. I. et al. Predisposition for cholera of individuals with O blood group. Possible evolutionary significance. *Am. J. Epidemiol.* **121**, 791–796 (1985).
16. Barua, D. & Paguio, A. S. ABO blood groups and cholera. *Ann. Hum. Biol.* **4**, 489–492 (1977).
17. Chaudhuri, A. & De, S. Cholera and blood-groups. *Lancet* **2**, 404 (1977).

18. Swerdlow, D. L. et al. Severe life-threatening cholera associated with blood group O in Peru: implications for the Latin American epidemic. *J. Infect. Dis.* **170**, 468–472 (1994).
19. Harris, J. B. et al. Blood group, immunity, and risk of infection with *Vibrio cholerae* in an area of endemicity. *Infect. Immun.* **73**, 7422–7427 (2005).
20. Harris, J. B. et al. Susceptibility to *Vibrio cholerae* infection in a cohort of household contacts of patients with cholera in Bangladesh. *PLoS Negl. Trop. Dis.* **2**, e221 (2008).
21. Heggelund, J. E. et al. High-resolution crystal structures elucidate the molecular basis of cholera blood group dependence. *PLoS Pathog.* **12**, e1005567 (2016).
22. Heggelund, J. E. et al. Both El Tor and classical cholera toxin bind blood group determinants. *Biochem. Biophys. Res. Commun.* **418**, 731–735 (2012).
23. Holmner, A. et al. Novel binding site identified in a hybrid between cholera toxin and heat-labile enterotoxin: 1.9 Å crystal structure reveals the details. *Structure* **12**, 1655–1667 (2004).
24. Bennun, F. R., Roth, G. A., Monferran, C. G. & Cumar, F. A. Binding of cholera toxin to pig intestinal mucosa glycosphingolipids: relationship with the ABO blood group system. *Infect. Immun.* **57**, 969–974 (1989).
25. Wands, A. M. et al. Fucosylated molecules competitively interfere with cholera toxin binding to host cells. *ACS Infect. Dis.* **4**, 758–770 (2018).
26. Prudden, A. R. et al. Synthesis of asymmetrical multiantennary human milk oligosaccharides. *Proc. Natl Acad. Sci. USA* **114**, 6954–6959 (2017).
27. Heim, J. B., Hodnik, V., Heggelund, J. E., Anderluh, G. & Krengel, U. Crystal structures of cholera toxin in complex with fucosylated receptors point to importance of secondary binding site. *Sci. Rep.* **9**, 12243 (2019).
28. Garber, J. M., Hennet, T. & Szymanski, C. M. Significance of fucose in intestinal health and disease. *Mol. Microbiol.* **115**, 1086–1093 (2021).
29. Wands, A. M. et al. Fucosylation and protein glycosylation create functional receptors for cholera toxin. *eLife* **4**, e09545 (2015).
30. Blanco, L. P. & DiRita, V. J. Bacterial-associated cholera toxin and GM1 binding are required for transcytosis of classical biotype *Vibrio cholerae* through an in vitro M cell model system. *Cell Microbiol* **8**, 982–998 (2006).
31. Sethi, A. et al. Cell type and receptor identity regulate cholera toxin subunit B (CTB) internalization. *Interface Focus* **9**, 20180076 (2019).
32. Sojitra, M. et al. Genetically encoded multivalent liquid glycan array displayed on M13 bacteriophage. *Nat. Chem. Biol.* **17**, 806–816 (2021).
33. Yanagisawa, M., Ariga, T. & Yu, R. K. Cholera toxin B subunit binding does not correlate with GM1 expression: a study using mouse embryonic neural precursor cells. *Glycobiology* **16**, 19g–22g (2006).
34. Bakker, H., Ashikov, A., Routier, F. H. & Gerardy-Schahn, R. in *Handbook of Glycosyltransferases and Related Genes* Ch. 124 (eds Taniguchi, N. et al.) 1403–1412 (Springer, 2014).
35. Foulquier, F. et al. TMEM165 deficiency causes a congenital disorder of glycosylation. *Am. J. Hum. Genet* **91**, 15–26 (2012).
36. Togayachi, A. & Narimatsu, H. in *Handbook of Glycosyltransferases and Related Genes* Ch. 29 (eds Taniguchi, N. et al.) 311–320 (Springer, 2014).
37. Togayachi, A. & Narimatsu, H. in *Handbook of Glycosyltransferases and Related Genes* Ch. 9 (eds Taniguchi, N. et al.) 89–100 (Springer, 2014).
38. Lin, C. H. et al. Enhanced expression of β3-galactosyltransferase 5 activity is sufficient to induce in vivo synthesis of extended type 1 chains on lactosylceramides of selected human colonic carcinoma cell lines. *Glycobiology* **19**, 418–427 (2009).
39. Lin, R. J. et al. *B3GALT5* knockout alters gycosphingolipid profile and facilitates transition to human naive pluripotency. *Proc. Natl Acad. Sci. USA* **117**, 27435–27444 (2020).
40. Isshiki, S. et al. Cloning, expression, and characterization of a novel UDP-galactose: β-*N*-acetylglucosamine β-galactosyltransferase (β3Gal-T5) responsible for synthesis of type 1 chain in colorectal and pancreatic epithelia and tumor cells derived therefrom. *J. Biol. Chem.* **274**, 12499–12507 (1999).
41. Groth, T., Diehl, A. D., Gunawan, R. & Neelamegham, S. GlycoEnzOnto: a glycoenzyme pathway and molecular function ontology. *Bioinformatics* **38**, 5413–5420 (2022).
42. Ancheta, L. R., Shramm, P. A., Bouajram, R., Higgins, D. & Lappi, D. A. Streptavidin–saporin: converting biotinylated materials into targeted toxins. *Toxins* **15**, 181 (2023).
43. Stirpe, F. et al. Ribosome-inactivating proteins from the seeds of *Saponaria officinalis* L. (soapwort), of *Agrostemma githago* L. (corn cockle) and of *Asparagus officinalis* L. (asparagus), and from the latex of *Hura crepitans* L. (sandbox tree). *Biochem. J.* **216**, 617–625 (1983).
44. Lee, L., Abe, A. & Shayman, J. A. Improved inhibitors of glucosylceramide synthase. *J. Biol. Chem.* **274**, 14662–14669 (1999).
45. Singla, A. et al. Cholera intoxication of human enteroids reveals interplay between decoy and functional glycoconjugate ligands. *Glycobiology* **33**, 801–816 (2023).
46. Moss, J., Fishman, P. H., Manganiello, V. C., Vaughan, M. & Brady, R. O. Functional incorporation of ganglioside into intact cells—induction of choleragen responsiveness. *Proc. Natl Acad. Sci. USA* **73**, 1034–1037 (1976).
47. Gilbert, L. A. et al. Genome-scale CRISPR-mediated control of gene repression and activation. *Cell* **159**, 647–661 (2014).
48. Tringali, C. et al. Modification of sialidase levels and sialoglycoconjugate pattern during erythroid and erytroleukemic cell differentiation. *Glycoconj. J.* **24**, 67–79 (2007).
49. Arumugam, S. et al. Ceramide structure dictates glycosphingolipid nanodomain assembly and function. *Nat. Commun.* **12**, 3675 (2021).
50. Chinnapen, D. J. et al. Lipid sorting by ceramide structure from plasma membrane to ER for the cholera toxin receptor ganglioside GM1. *Dev. Cell* **23**, 573–586 (2012).
51. Kenworthy, A. K. et al. Cholera toxin as a probe for membrane biology. *Toxins* **13**, 543 (2021).
52. Madunic, K. et al. Specific (sialyl-)Lewis core 2 *O*-glycans differentiate colorectal cancer from healthy colon epithelium. *Theranostics* **12**, 4498–4512 (2022).
53. Robbe, C., Capon, C., Coddeville, B. & Michalski, J. C. Structural diversity and specific distribution of *O*-glycans in normal human mucins along the intestinal tract. *Biochem. J.* **384**, 307–316 (2004).
54. Goto, Y. et al. Innate lymphoid cells regulate intestinal epithelial cell glycosylation. *Science* **345**, 1254009 (2014).
55. Carroll, D. J. et al. Interleukin-22 regulates *B3GNT7* expression to induce fucosylation of glycoproteins in intestinal epithelial cells. *J. Biol. Chem.* **298**, 101463 (2022).
56. Pham, T. A. et al. Epithelial IL-22RA1-mediated fucosylation promotes intestinal colonization resistance to an opportunistic pathogen. *Cell Host Microbe* **16**, 504–516 (2014).
57. Pickard, J. M. et al. Rapid fucosylation of intestinal epithelium sustains host–commensal symbiosis in sickness. *Nature* **514**, 638–641 (2014).

58. Pickard, J. M. & Chervonsky, A. V. Intestinal fucose as a mediator of host–microbe symbiosis. *J. Immunol.* **194**, 5588–5593 (2015).
59. Meng, D. et al. Bacterial symbionts induce a FUT2-dependent fucosylated niche on colonic epithelium via ERK and JNK signaling. *Am. J. Physiol. Gastrointest. Liver Physiol.* **293**, G780–G787 (2007).
60. Muraoka, W. T. & Zhang, Q. Phenotypic and genotypic evidence for L-fucose utilization by *Campylobacter jejuni*. *J. Bacteriol.* **193**, 1065–1075 (2011).
61. Stahl, M. et al. L-Fucose utilization provides *Campylobacter jejuni* with a competitive advantage. *Proc. Natl Acad. Sci. USA* **108**, 7194–7199 (2011).
62. Staib, L. & Fuchs, T. M. Regulation of fucose and 1,2-propanediol utilization by *Salmonella enterica* serovar Typhimurium. *Front. Microbiol* **6**, 1116 (2015).
63. Ruiz-Palacios, G. M., Cervantes, L. E., Ramos, P., Chavez-Munguia, B. & Newburg, D. S. *Campylobacter jejuni* binds intestinal H(O) antigen (Fucα1, 2Galβ1, 4GlcNAc), and fucosyloligosaccharides of human milk inhibit its binding and infection. *J. Biol. Chem.* **278**, 14112–14120 (2003).
64. Chessa, D., Winter, M. G., Jakomin, M. & Bäumler, A. J. *Salmonella enterica* serotype Typhimurium Std fimbriae bind terminal α(1,2) fucose residues in the cecal mucosa. *Mol. Microbiol.* **71**, 864–875 (2009).
65. Barra, J. L., Monferran, C. G., Balanzino, L. E. & Cumar, F. A. *Escherichia coli* heat-labile enterotoxin preferentially interacts with blood group A-active glycolipids from pig intestinal mucosa and A- and B-active glycolipids from human red cells compared to H-active glycolipids. *Mol. Cell. Biochem.* **115**, 63–70 (1992).
66. Balanzino, L. E., Barra, J. L., Galván, E. M., Roth, G. A. & Monferran, C. G. Interaction of cholera toxin and *Escherichia coli* heat-labile enterotoxin with glycoconjugates from rabbit intestinal brush border membranes: relationship with ABH blood group determinants. *Mol. Cell. Biochem.* **194**, 53–62 (1999).
67. Galván, E. M., Roth, G. A. & Monferran, C. G. Participation of ABH glycoconjugates in the secretory response to *Escherichia coli* heat-labile toxin in rabbit intestine. *J. Infect. Dis.* **180**, 419–425 (1999).
68. Galván, E. M., Diema, C. D., Roth, G. A. & Monferran, C. G. Ability of blood group A-active glycosphingolipids to act as *Escherichia coli* heat-labile enterotoxin receptors in HT-29 cells. *J. Infect. Dis.* **189**, 1556–1564 (2004).
69. Galván, E. M., Roth, G. A. & Monferran, C. G. Functional interaction of *Escherichia coli* heat-labile enterotoxin with blood group A-active glycoconjugates from differentiated HT29 cells. *FEBS J.* **273**, 3444–3453 (2006).
70. Holmner, A., Askarieh, G., Okvist, M. & Krengel, U. Blood group antigen recognition by *Escherichia coli* heat-labile enterotoxin. *J. Mol. Biol.* **371**, 754–764 (2007).
71. Marionneau, S. et al. Norwalk virus binds to histo-blood group antigens present on gastroduodenal epithelial cells of secretor individuals. *Gastroenterology* **122**, 1967–1977 (2002).
72. Huang, P. et al. Noroviruses bind to human ABO, Lewis, and secretor histo-blood group antigens: identification of 4 distinct strain-specific patterns. *J. Infect. Dis.* **188**, 19–31 (2003).
73. Lindesmith, L. et al. Human susceptibility and resistance to Norwalk virus infection. *Nat. Med.* **9**, 548–553 (2003).
74. Harrington, P. R., Vinjé, J., Moe, C. L. & Baric, R. S. Norovirus capture with histo-blood group antigens reveals novel virus–ligand interactions. *J. Virol.* **78**, 3035–3045 (2004).
75. Huang, P. et al. Norovirus and histo-blood group antigens: demonstration of a wide spectrum of strain specificities and classification of two major binding groups among multiple binding patterns. *J. Virol.* **79**, 6714–6722 (2005).
76. Borén, T., Falk, P., Roth, K. A., Larson, G. & Normark, S. Attachment of *Helicobacter pylori* to human gastric epithelium mediated by blood group antigens. *Science* **262**, 1892–1895 (1993).
77. Ilver, D. et al. *Helicobacter pylori* adhesin binding fucosylated histo-blood group antigens revealed by retagging. *Science* **279**, 373–377 (1998).
78. Ikehara, Y. et al. Polymorphisms of two fucosyltransferase genes (Lewis and Secretor genes) involving type I Lewis antigens are associated with the presence of anti-*Helicobacter pylori* IgG antibody. *Cancer Epidemiol. Biomark. Prev.* **10**, 971–977 (2001).
79. Aspholm-Hurtig, M. et al. Functional adaptation of BabA, the *H. pylori* ABO blood group antigen binding adhesin. *Science* **305**, 519–522 (2004).
80. Hage, N. et al. Structural basis of Lewis^b antigen binding by the *Helicobacter pylori* adhesin BabA. *Sci. Adv.* **1**, e1500315 (2015).

Methods

EGCase expression and purification

Escherichia coli BL21(DE3) cells were transformed with a pET30 plasmid encoding *Rhodococcus triatomae* EGCase I (RhtrECI)[81]. A 1-L culture of the transformed cells was induced with 0.1 mM IPTG at 16 °C for 18–20 h with continuous shaking at 200 r.p.m. Cells were harvested by centrifugation (8,980*g* for 30 min) and resuspended in 40 ml of lysis buffer (50 mM Tris pH 7.5 containing 300 mM NaCl and 0.1% Triton X-100). Cells were disrupted by sonication for 5 min (60 amplitude with 10-s pulse on and 30-s pulse off). The supernatant was cleared by centrifugation (150,700*g* at 4 °C for 1 h) and then loaded onto a 2-ml Ni-NTA column (Qiagen) pre-equilibrated with ten column volumes of 50 mM Tris pH 7.5 containing 300 mM NaCl. EGCase I was eluted with 250 mM imidazole and dialyzed with TBS (50 mM Tris-HCl pH 7.5 containing 150 mM NaCl). The homogeneity of purified EGCase I was analyzed by SDS–PAGE.

Cell culture

Colo205 cells (American Type Culture Collection (ATCC)) were maintained in RPMI-1640 medium (Gibco) supplemented with 10% FBS (v/v) and 1% penicillin–streptomycin (Sigma). HEK293T/17 cells (ATCC) were maintained in DMEM supplemented with 20% FBS. Both cell lines were maintained at 37 °C, 5% CO_2 in a water-saturated environment and were not used past passage number 50 or 15, respectively. The Countess automated cell counter (Life Technologies) was used for cell counting.

Flow cytometry

Colo205 cells were seeded in a 10-cm tissue culture plate at a density of 2×10^5 cells per ml and cultured before experiments for 48 h or for 72 h when seeded at a density of 1×10^5 cells per ml. For experiments requiring the inhibition of glucosylceramide GSL biosynthesis, 1×10^5 cells per ml were plated with the addition of P4 inhibitor at a final concentration of 1 µM and cultured for 72 h. Medium containing floating cells was collected and 2 ml of 10 mM EDTA in DPBS was added to adherent Colo205 cells before incubating for 5 min at 37 °C. Adherent cells were then dislodged by gentle resuspension and then combined with previously harvested floating cell population. Cells were centrifuged at 500*g* for 3 min and EDTA was removed by aspiration. The cells were resuspended in DPBS containing 0.1% (w/v) BSA in Dulbecco's PBS (DPBS/BSA) and 3.5×10^5 cells were added per well to a V-bottom plate (Costar, cat. no. 3897). Cells were pelleted by centrifugation at 730*g* for 5 min at 4 °C and washed twice by resuspension in 200 µl of cold DPBS/BSA. Cells were incubated for 30 min on ice with 50 µl of the indicated concentration of unlabeled CTB for dose responses, 50 µl of 1 µg ml^{-1} unlabeled CTB or 50 µl of the indicated lectin or antibody diltuions (Supplementary Table 1). Cells were then washed twice with 200 µl of cold DPBS/BSA and incubated for 30 min on ice with the respective secondary antibodies. After two washes, cells were subjected to flow cytometric analysis using the FACSCalibur flow cytometer (BD Biosciences, University of Texas (UT) Southwestern Flow Cytometry Core facility). Flow cytometry data were analyzed using the FlowJo software (BD Biosciences). Single cells were gated on the basis of forward versus side scatter. Dead cells were excluded on the basis of PI staining on the FL3 channel and the fluorescence intensity of the live population was determined on the FL4 emission channel. The gating strategy is depicted in Supplementary Fig. 1.

CRISPR screen

The human Brunello genome-wide CRISPR KO pooled library[82] (gift from D. Root and J. Doench; Addgene, cat. no. 73178) was amplified by electroporation into Stbl4 electrocompetent cells (Thermo Fisher Scientific, cat. no. 11635-018) according to the manufacturer's instructions.

To generate lentivirus, 7.5×10^6 low-passage HEK293T/17 cells were plated on each of ten 15-cm dishes in 30 ml of complete medium. After 24 h, 48 µl of TransIT-293 transfection reagent (Mirus Bio, cat. no. MIR 2704) diluted with 1,300 µl of serum-free medium (SFM) was incubated for 5 min at room temperature and then combined with a mix of 8 µg of purified plasmid library DNA, 8 µg of psPAX2 packaging plasmid DNA and 1 µg of pMD2.G envelope plasmid DNA (gifts from D. Trono; Addgene, plasmid nos. 12260 and 12259, respectively). After incubating for 30 min, the mix was evenly split and added dropwise to each plate of HEK293T/17 cells. Viral supernatant was collected 72 h after infection, filtered through a 0.4-µm filter and then titrated in six-well plates containing 2×10^6 Colo205 cells to determine the amount of virus needed to infect cells at a multiplicity of infection of 0.3. Briefly, cells were resuspended in media with 8 µg ml^{-1} polybrene and increasing volumes of lentivirus (0, 50, 100, 200, 500 or 1,000 µl brought up to 2 ml with complete medium). Cells were then centrifuged at 1,000*g* for 2 h at 33 °C, and then transferred to an incubator and maintained at 37 °C in 5% CO_2 for 16 h. Each well (containing ~4×10^6 cells) was then harvested and 2.5×10^4 cells were plated in triplicate in wells of a white 96-well plate with a clear bottom (Costar Laboratories). Then, 24 h after passaging, library-expressing cells were selected with 5 µg ml^{-1} puromycin. Next, 48 h after selection, cell death was measured using the Cell Titer-Glo 2.0 (CTG) luminescent cell viability assay kit (Promega) and the virus volume condition (100 µl) resulting in ~30% viability was selected for use.

A total of 2×10^6 Colo205 cells were spinfected in each well of eight six-well plates (9.6×10^7 cells in total to ensure 300× coverage of the pooled library after selection) with 100 µl of virus brought up to 2 ml with complete medium containing 8 µg ml^{-1} polybrene, determined by titration as described above. Then, 24 h after infection, cells were harvested, resuspended in fresh medium and expanded in 20 15-cm dishes. Next, 24 h after passaging, library-expressing cells were selected with 5 µg ml^{-1} puromycin. Cells were harvested at 0 and 14 days after puromycin selection, consistently maintaining 300× library coverage. After harvesting on day 14, cells were centrifuged at 500*g* for 3 min at 4 °C and washed twice in DPBS. An input control population was set aside and the remaining cells were resuspended in DPBS containing 2% FBS (FACS buffer). Then, 7×10^6 cells were added to each of four round-bottom polystyrene 12 × 75-mm tubes (Corning, cat. no. 352008) and then washed twice by resuspension in 4 ml of cold FACS buffer. Cells were then incubated for 30 min on ice with 1 ml of biotin–CTB (Supplementary Table 1). After two washes, cells were incubated with 1 ml of fluorescein (DTAF) streptavidin. After a final two washes, cells were sorted and the top and bottom 1% fluorescent cells were collected using the FACSAria flow cytometer (BD Biosciences, UT Southwestern Flow Cytometry Core facility).

Immediately after sorting, both the input and the sorted cell populations were pelleted and genomic DNA (gDNA) was isolated from each using the blood and cell culture DNA Maxi kit (Qiagen, cat. no. 13362) according to the manufacturer's instructions. To amplify sgRNA sequences for next-generation sequencing (NGS), four parallel 100-µl PCR reactions were initially run for each condition and pooled. Each 100-µl PCR reaction contained 1–2 µg of gDNA, Ex Taq polymerase (Takara Bio, cat. no. RR01CM) and the PCR1 primer pair (Supplementary Table 2). Amplified DNA was then indexed and barcoded for NGS in another PCR reaction including 5 µl of DNA from the initial PCR, Ex Taq polymerase and pooled P5 and barcoded P7 primers (Supplementary Table 2). DNA was then pooled and purified for sequencing using AMPure XP beads (Agencourt). Next, 300 µl of pooled PCR product was mixed with 150 µl of beads and incubated for 5 min to remove gDNA. Beads bound to gDNA were pelleted on the DynaMag-2 Magnet (Invitrogen), and the supernatant was then mixed with 540 µl of fresh beads and incubated for 5 min to bind the PCR products. After discarding the supernatant, beads were washed twice with 1 ml of 70% ethanol and then dried for approximately 5 min. Bound DNA was eluted from the beads using 300 µl of sterile, nuclease-free water. Samples were sequenced using the Illumina NextSeq 500 with the read configuration

as single-end 75-bp reads at the UT Southwestern McDermott NGS core. Data were analyzed with MAGeCK[83]. The gene set enrichment analyses of the identified genes were performed with WebGestalt[84]. The Manhattan dot plots of the screen results were drawn with R package qqman (version 0.1.8)[85].

Construction of cell lines

OE plasmids for the rescue of *B3GALT5*- and *B3GNT5*-KOs were generated by Gibson cloning using primers designed using the NEBuilder software from New England Biolabs (NEB) to amplify the open reading frame (ORF) of each gene (Origene, cat. nos. RC211183L3 and RC206965L3, respectively) while introducing a 1-bp change to the protospacer-adjacent motif (PAM) sequence that does not result in a change to amino acid sequence (Supplementary Table 2). Amplification was performed using the Q5 high-fidelity 2X master mix (NEB, cat. no. M0492S) according to the manufacturer's instructions. Amplified ORFs were then purified using the MinElute PCR purification kit (Qiagen, cat. no. 28004) according to the manufacturer's instructions. For *B3GALT5*-KO + mut OE, we first identified the catalytic residues of B3GALT5 (D156 and D243) by aligning an AlphaFold[86] model of human B3GALT5 with the experimentally determined crystal structure of B3GNT2 (ref. 87). A gBlock gene fragment encoding the *B3GALT5* gene was designed to include the point substitutions D156A and D243A and the same 1-bp change to the PAM sequence as in the WT rescue plasmid. Purified PCR products of the WT *B3GALT5* gene or gBlock encoding the mutated *B3GALT5* gene were ligated using the HiFi DNA Assembly master mix (NEB, cat. no. E2621S) into a blasticidin resistance-encoding lentiviral vector (Addgene, plasmid no. 52962) cut with BamHI-HF and AfeI (NEB, cat. nos. R3136S and R0652S, respectively) according to the manufacturer's guidelines. Plasmids were transformed into Stbl3 competent cells according to the manufacturer's instructions and bacterial clones expressing the sequence-validated plasmid were expanded for maxiprep using the ZymoPure II maxiprep kit (Zymo Research, cat. no. D4204). Lentivirus was prepared as described for the CRISPR screen but scaled for production in individual 10-cm dishes. Then, 1 ml of lentivirus was added to 1×10^6 Colo205 cells in 2 ml of complete RPMI-1640 medium in each well of a six-well plate for transduction. Polybrene was added to a final concentration of 8 μg ml^{-1} and cells were then spinfected at 33 °C for 2 h. Then, 16 h after infection, cells were harvested, resuspended in fresh medium and expanded in 10-cm dishes. Next, 24 h after passaging, plasmid-expressing cells were selected with 5 μg ml^{-1} blasticidin. The resulting polyclonal populations were used for experiments using *B3GNT5*-KO + OE, *B3GALT5*-KO + OE, and *B3GALT5*-KO + mut OE cells.

All-in-one CRISPR KO plasmid lentivirus for the expression of Cas9 and predesigned sgRNAs targeting *B3GALT5*, *B3GNT5*, *SLC35C1* or a non-targeting scramble control sgRNA (Sigma, cat. nos. HSPD0000061666, HSPD0000119328, HSPD0000095207 or NegativeControl1, respectively) were used to spinfect Colo205 cells as described above but using 200 μl of virus and selecting for plasmid-expressing cells with 5 μg ml^{-1} puromycin. Monoclonal populations were obtained using FACS in a sterile environment (UT Southwestern Flow Cytometry Core) to collect single, green fluorescent protein-positive cells in each well of a 96-well tissue culture plate containing 200 μl of complete medium supplemented with extra FBS (20% v/v total). To generate dKO cell lines, the lentiGuide-neo plasmid was cut with BsmBI and dephosphorylated before gel purification. Oligos encoding the sgRNA sequence for each gene (Supplementary Table 2) were phosphorylated, annealed and ligated into the lentiGuide-neo plasmid. Plasmids were then transformed into Stbl3 bacterial cells according to the manufacturer's instructions. Lentivirus generation and delivery were performed as with the OE plasmids, selecting plasmid-expressing cells with 400 μg ml^{-1} G418. Monoclonal populations of dKO cells were isolated by limiting dilution.

To sequence the CRISPR-targeted genes, gDNA was isolated from 5×10^6 Colo205 cells using the blood and cell culture DNA Maxi kit (Qiagen, cat. no. 13362) according to the manufacturer's instructions. The respective gene targets were amplified by PCR using Ex Taq polymerase (Takara Bio, cat. no. RR01CM) according to the manufacturer's instructions. The forward and reverse primers for each sequenced gene are listed in Supplementary Table 2. The PCR products were purified using the NucleoSpin gel and PCR clean-up mini kit (Macherey-Nagel, cat. no. 740609.50) according to the manufacturer's instructions. Purified DNA was ligated into a pGEM-T Easy prelinearized vector (Promega, cat. no. A1360) and transformed into DH5α competent cells. Plasmids were extracted from single colonies and then submitted to the UT Southwestern Sanger Sequencing Core. Sequence data are presented in Supplementary Table 3. For all KO cell lines, except the *B3GALT5* + *SLC35C1*-dKO, two different indels were identified, each in duplicate or triplicate. For KO of *SLC35C1* in the *B3GALT5*-KO line, four separate clones harbored the same *SLC35C1* indel. Loss of SLC35C1 activity was inferred by the complete loss of anti-Le^x and *Aleuria aurantia* lectin (AAL) binding to these cells.

Measurement of CTB internalization

A total of 2.5×10^3 Colo205 cells in 90 μl of serum-free RPMI-1640 medium (SFM) were plated in each well of a white-walled, 96-well clear-bottom plate (Costar Laboratories). Cells were cultured for 72 h in SFM with 10 μl of CTB–saporin or saporin alone (0, 1.25, 2.5 and 12.5 μg ml^{-1} final concentrations) in triplicate at 5% CO_2 at 37 °C. CTB–saporin complexes were prepared according to the manufacturer's instructions. Briefly, 7 μl of 1.8 mg ml^{-1} biotinylated CTB was combined with 4.2 μl of 1.6 mg ml^{-1} streptavidin–saporin (Advanced Targeting Systems, IT-27) and incubated at room temperature for 20 min. The mixture was then diluted with SFM to a volume of 100 μl to generate a 125 μg ml^{-1} CTB–saporin solution and serially diluted to generate 25 and 12.5 μg ml^{-1} CTB–saporin solutions. After incubating cells with 10 μl of the respective CTB–saporin solutions or saporin alone for 72 h, cell death was measured using the CTG luminescent cell viability assay kit (Promega).

Measurement of cAMP

A total of 2.5×10^4 Colo205 cells in 20 μl of SFM were plated in each well of a white 96-well plate with a clear bottom (Costar Laboratories). Triplicate wells were incubated with 10 μl of BFA (1 μg ml^{-1}) in SFM supplemented with $MgCl_2$ (50 mM), IBMX (500 μM) and Ro-20-1764 (100 μM) (complete induction buffer). All other wells were treated with 10 μl of vehicle control. After 30 min, BFA-treated or vehicle-treated control cells were treated with 10 μl of the indicated concentration of CT diluted in induction buffer in triplicate at 5% CO_2 at 37 °C for 90 min. Forskolin (10 μM final concentration) was added to vehicle-treated control wells in triplicate and incubated at 5% CO_2 at 37 °C for 15 min and then 15 min at room temperature before measurement of cAMP accumulation. Accumulated cAMP was measured using the cAMP-Glo Max assay kit (Promega) according to the manufacturer's instructions with modification to incubation times (30-min incubation with cAMP-Glo ONE buffer and 20-min incubation with the kinase-Glo buffer). Luminescence values were inversely proportional to cAMP levels. Inverse cAMP-Glo values were first corrected for differences in cells plated per well for each cell line. The number of cells per well was measured in vehicle control-treated wells using the CTG reagent, which was added to vehicle-treated control wells in triplicate for each cell line 15 min after the addition of cAMP-Glo Max Assay kit ONE buffer. CTG-corrected cAMP values were then normalized to the maximum signal in scramble control cells.

Lectin blot and immunoblot analyses

Colo205 cells (4×10^6) were lysed in 200 μl of radioimmunoprecipitation (RIPA) buffer (50 mM Tris-HCl pH 8, 150 mM NaCl, 0.01% (v/v) SDS, 0.5% (v/v) sodium deoxycholate, 1% (v/v) IGEPAL CA-630 and

1× protease inhibitor). Protein content was quantified with a BCA assay kit (Thermo Fisher Scientific) against a BSA standard curve for normalization. For protease digestions, 20 µg of lysate was incubated with 500 µg ml^{-1} proteinase K in RIPA buffer for 48 h at 37 °C. EGCase digestions were performed by incubating 20 µg of lysate with 40 µg of enzyme in 50 mM sodium acetate buffer (pH 5.2) supplemented with 0.2% Triton X-100 overnight at 37 °C. Then, 20 µg of lysate was denatured in 1× SDS loading dye (250 mM Tris-HCl pH 6.8, 0.08% (w/v) SDS, 0.0004% (w/v) bromophenol blue, 40% (v/v) glycerol and 10 mM DTT) for 10 min at 95 °C for all conditions. The samples were resolved on a 4–20% stain-free gradient SDS–PAGE gel (Bio-Rad Laboratories) and activated for 1 min using the ChemiDoc MP Imaging system (Bio-Rad Laboratories). Activated protein was transferred to a PVDF membrane (ED Millipore) using the Trans-Blot SD semidry transfer cell (Bio-Rad Laboratories) according to the manufacturer's guidelines at 15 V for 45 min and total protein stain was imaged using the ChemiDoc MP. After blocking at room temperature for 1 h, membranes were probed overnight at 4 °C. Membranes probed with CTB and anti-Le^x (Supplementary Table 1) were blocked and incubated in 5% nonfat milk prepared in 1× TBS containing 0.05% (v/v) Tween-20 (TBS-T). The horseradish peroxidase signal was detected using the SuperSignal West Femto maximum-sensitivity substrate diluted in SuperSignal West Pico PLUS chemiluminescent substrate (Thermo Fisher Scientific, cat. nos. 34096 and 34580, respectively) according to the manufacturer's recommendations and the ChemiDoc MP Imaging system (Bio-Rad Laboratories). When probing with AAL (Supplementary Table 1), membranes were blocked and incubated with 1× Carbo-Free blocking solution (Vector Laboratories, cat. no. SP-5040-125) prepared in water. AAL blots were imaged after washing with 1× TBS-T using the Typhoon FLA 9500 gel imaging scanner (GE Life Sciences).

Total GSL isolation

Preparation of glycolipids from whole cells was carried out using previously described methods[88]. Pellets of cells were disrupted with probe sonication between extraction of the total lipids with 4:8:3 chloroform, methanol and water (CMW). The mixture was bath-sonicated in ice before centrifugation to pellet the proteinaceous material to the bottom. The supernatant was then removed to a clean glass tube. Fresh aliquots of CMW were added two more times with sonication, each time removing the supernatant. The combined supernatant, which contained the crude lipid extraction, was then dried down, reconstituted in 0.5 M NaOH in methanol (methanol and water 95:5 v/v), sonicated to redissolve the lipids and incubated at 37 °C overnight to saponify the phosphoglycerolipids. The next day, an equal volume of 5% acetic acid was added to the reaction to neutralize and halt saponification and the sample was desalted on a tC18 solid-phase extraction (SPE) cartridge (Waters), resulting in the isolated GSL material. Free fatty acids were removed from the sample by drying the GSL material by addition and removal of hexane. The sample was thoroughly dried before further analysis.

For Extended Data Fig. 6a, GSLs were incubated overnight with EGCase II in 50 mM sodium acetate buffer (pH 5.0). Then, the glycans were isolated by loading the mixture on a C18 SPE cartridge and eluting using 5% acetic acid solution. This solution was lyophilized and incubated overnight with procainamide in the presence of sodium cyanoborohydride and acetic acid in DMSO. This mixture was then analyzed using a Waters Acquity ultrahigh-performance LC (UPLC) system equipped with a Waters Acquity UPLC amide BEH column. The UHPLC system was coupled to a Waters Synapt XS quadrupole time-of-flight MS instrument with an ESI source operated in positive ion mode. MassLynx software (version 4.2, Waters Corporation) was used for molecular feature extraction and data processing. Identities were confirmed by matching accurate mass, retention time and observation of the signature ion of Hex(2)-PC in MS/MS data (m/z = 562.31).

Nonacid GSL isolation

B3GNT5-KO + OE cells (1 × 10^9 cells) were first extracted at 70 °C with methanol and thereafter extracted three times with 33% methanol in chloroform and three times with 67% methanol in chloroform[89]. The extracts were combined, dried and subjected to mild alkaline methanolysis, followed by dialysis. Then, the extracts were acetylated and the acetylated lipids were separated on a silicic acid column, eluting first with dichloromethane to remove nonpolar material. Thereafter, the acetylated lipids were eluted with 5% and 7.5% methanol (by volume) in chloroform. Finally, sphingomyelin was eluted with 75% methanol in chloroform and pure methanol. The fractions eluted with 5% and 7.5% methanol in chloroform were combined and deacetylated using 0.2 M KOH in methanol followed by dialysis. Thereafter, acid and nonacid GSLs were separated on a DEAE-Sepharose column, yielding 3.2 mg of nonacid GSLs. This material was used for the experiments presented in Fig. 3f and the LC–ESI/MS analysis presented in Extended Data Fig. 6b,c.

EGCase digestion and LC–ESI/MS of nonacid GSLs

Before MS analysis, the nonacid GSLs were digested with EGCase I (TCI R0240) to remove the ceramide part. The GSLs (50 µg) were resuspended in 100 µl of 0.05 M sodium acetate buffer (pH 5.0) containing 120 µg of sodium cholate and sonicated briefly. Thereafter, 1 mU of enzyme was added and the mixture was incubated at 37 °C for 2 h. The reaction was stopped by the addition of CMW at a final proportion of 8:4:3 (by volume). The oligosaccharide-containing upper phase thus obtained was separated from detergent on a Sep-Pak QMA cartridge (Waters) and the eluant containing the oligosaccharides was dried.

The GSL-derived oligosaccharides were resuspended in 50 µl of water and analyzed by LC–ESI/MS as described previously[90]. The oligosaccharides were separated on a column (100 × 0.250 mm) packed in-house with 5-µm porous graphite particles. An autosampler, HTC-PAL (equipped with a cheminert valve (0.25-mm bore) and a 2-µl loop) was used for sample injection. An Agilent 1100 binary pump delivered a flow of 250 µl min^{-1}, which was split down in an 1/16-inch microvolume-T (0.15-mm bore) by a 50-cm (50-µm inner diameter) fused silica capillary before the injector of the autosampler, allowing approximately 3–5 µl min^{-1} through the column. The oligosaccharides (3 µl) were injected onto the column and eluted with an acetonitrile gradient (mobile phase A, 10 mM ammonium bicarbonate; mobile phase B, 10 mM ammonium bicarbonate in 80% acetonitrile). The gradient (0–45% B) was eluted for 46 min, followed by a wash step with 100% B and equilibration of the column for 24 min. A 30-cm (50-µm inner diameter) fused silica capillary was used as a transfer line to the ion source.

The oligosaccharides were analyzed in negative ion mode on an LTQ (linear quadrupole ion trap) MS instrument from Thermo Electron. The IonMax standard ESI source on the LTQ MS instrument was equipped with a stainless-steel needle kept at −3.5 kV. Compressed air was used as nebulizer gas. The heated capillary was kept at 270 °C and the capillary voltage was −50 kV. A full scan (m/z 380–2,000, two microscans, maximum of 100 ms and target value of 30,000) was performed, followed by data-dependent MS^2 scans of the three most abundant ions in each scan (two microscans, maximum of 100 ms and target value of 10,000). The threshold for MS^2 was set to 500 counts. The normalized collision energy was 35% and an isolation window of 3 m/z, an activation q = 0.25 and an activation time of 30 ms, was used. Data acquisition and processing were conducted with Xcalibur software (Versions 2.0.7 and 4.4).

Manual assignment of glycan sequences was performed on the basis of knowledge of mammalian biosynthetic pathways, with the assistance of the Glycoworkbench tool (version 2.1) and by comparison of retention times and MS^2 spectra of oligosaccharides from reference GSLs[90].

CT intoxication of cells treated with nonacid GSLs

For glycolipid add-back experiments, scramble control or *B3GALT5* + *B3GNT5*-dKO cells (1.5 × 10^6 in 1 ml of SFM) in Teflon-capped

glass vials were incubated with the indicated concentration of each lipid type or 1:2 chloroform and methanol (vehicle control) for 1 h of shaking at 4 °C. Cells were transferred to 1.5-ml Eppendorf tubes and washed twice with ice-cold dPBS. Cells were resuspended in SFM, and then CT intoxication was assayed as described above.

N-glycan and *O*-glycan release

Cell pellets were resuspended in ammonium bicarbonate and passed several times through a 23-gauge syringe to homogenize. Cells were further lysed with probe sonication and the lysate was denatured by adding 10 µl of denaturing buffer (NEB PNGase F kit, P0709) and heating at 100 °C for 5 min. Salts were removed with a prewashed 10-kDa MW cutoff (MWCO) filter and exchanged into 50 mM ammonium bicarbonate. Whole proteins were removed from the top of the MWCO filter and resuspended in 50 mM ammonium bicarbonate. *N*-glycans were released with PNGase F (NEB, P0709) for 20 h at 37 °C and the released *N*-glycans were isolated by passage through a prewashed 10-kDa MWCO filter. The remaining protein including *O*-linked glycans remained in the top of the filter and was removed before treatment with 1 M sodium borohydride in 50 mM sodium hydroxide. *O*-linked glycans were released with β-elimination at 45 °C overnight. The basic solution was neutralized with a 10% acetic acid solution, desalted through a packed Dowex column (50WX8-100, Sigma Aldrich) and then lyophilized. Borates were removed from the sample with repeated additions of 9:1 methanol and acetic acid under a nitrogen flow. The material was then resolubilized and passed through a C18 SPE cartridge to further purify the material before permethylation and analysis.

Permethylation and MS analysis

The GSL material was permethylated using previously described methods[91–93]. Briefly, dried samples were reconstituted in DMSO and treated with a mixture of methyl iodide in a DMSO–NaOH slurry. After quenching the reaction with the addition of water, the permethylated analytes were extracted from the solution by the addition of dichloromethane.

MS analysis was carried out by direct infusion MS or LC–MS. Permethylated glycans and glycolipids were reconstituted in a 50:50 methanol and water mixture containing 1 mM NaOH, which acted as a charge carrier. The solution was analyzed on a Thermo Orbitrap Fusion Tribrid MS instrument with direct infusion at a flow rate of 1–2 µl min^{-1} and analyzed in positive ion mode. An automated method that collects full MS spectra at 120,000 resolution followed by data-dependent MS/MS fragmentations (collision-induced dissociation (CID)) at 60,000 resolution was used to collect data for the GSLs. Data for the permethylated *N*-glycans and *O*-glycans were collected by LC–MS on a Thermo Orbitrap Fusion Tribrid MS instrument in line with an Ultimate 3000RSLCnano LC system. A 15-cm (75-µm inner diameter) commercial C18 column (Thermo Fisher, cat. no. 164568) filled with 3-µm C18 material was used for analysis. Injections of permethylated *N*-linked or *O*-linked glycans were carried out from low to high acetonitrile in water with 1 mM sodium acetate. The precursor ion scan was acquired at 120,000 resolution in the Orbitrap analyzer and precursors at 3 s were selected for MS/MS fragmentation (CID fragmentation) in the Orbitrap at 30,000 resolution.

CTB pulldown

For pulldown assays, *B3GALT5* + *B3GNT5*-dKO or *B3GALT5* + *SLC35C1*-dKO cells (1.5×10^7) were lysed in 500 µl of RIPA buffer. Lysates were diluted to 1.5 mg ml^{-1} in DPBS supplemented with 1× protease inhibitor. Then, 900 µl of lysates was added to a 1.5-ml LoBind microcentrifuge tube (Eppendorf, cat. no. 22431081) along with 2 µg ml^{-1} CTB–biotin and the samples were mixed by end-over-end rotation overnight at 4 °C. Next, 100 µl of Dynabeads M-280 streptavidin (Fisher, cat. no. 11205D) were washed with 500 µl of DPBS using a magnetic tube rack and then resuspended in 100 µl of DPBS with 1× protease inhibitor. Next, 100 µl of washed beads were added to the lysate and CTB–biotin mixture and then mixed by end-over-end rotation for 48 h at 4 °C. After 48 h, the beads were pelleted using a magnetic tube rack, gently washed three times with 1 ml of DPBS and then eluted with 20 µl of 2× SDS loading dye for 10 min at 95 °C. For MS analysis, the total supernatant was collected and loaded into a single well of a 4–20% stain-free SDS–PAGE gradient gel and run 1 cm into the gel. The gel was then stained with GelCode blue stain reagent (Thermo Scientific, cat. no. 24590) according to the manufacturer's instructions to visualize the band comprising the total protein mixture. This band was then destained, cut from the gel, diced into 1-mm^2 cubes and transferred to a 1.5-ml LoBind microcentrifuge tube for submission to the UT Southwestern MS core facility for total protein identification. Proteomics data were analyzed using Proteome Discoverer 3.0 and searched using the human protein database from UniProt. For western blot validation of the top hits identified by MS analysis, 10 µl of eluted samples were resolved on a 4–20% stain-free SDS–PAGE gradient gel, transferred to a PVDF membrane and probed with antibodies targeting FLOT1 or MUC1 (Supplementary Table 1).

Statistical analysis

Statistical analyses were performed using GraphPad Prism software (versions 9 and 10.0.1). Asterisks indicate significance as follows: $^*P < 0.05$, $^{**}P < 0.01$, $^{***}P < 0.001$ and $^{****}P < 0.0001$. No sample was excluded from data analysis and no blinding was used.

Biological materials

Hek293T/17 and parental Colo205 cells are available from the ATCC (CRL-11268 and CCL-222, respectively). Colo205 KO and rescue cell lines (*B3GALT5*-KO m1, *B3GALT5*-KO m2, *B3GALT5*-KO + WT OE, *B3GALT5*-KO + mut OE, *B3GNT5*-KO m1, *B3GNT5*-KO m2, *B3GNT5*-KO + OE, *B3GALT5* + *B3GNT5*-dKO, *SLC35C1*-KO and *B3GALT5* + *SLC35C1*-dKO cells) are available upon request to the corresponding author. The lentiGuideB3GNT5 and lentiGuideSLC35C1 CRISPR sgRNA plasmids and the *B3GNT5*, *B3GALT5* and mutated *B3GALT5*-OE plasmids are available from Addgene (cat. nos. 220867, 220868, 208380, 208381 and 220869).

Reporting summary

Further information on research design is available in the Nature Portfolio Reporting Summary linked to this article.

Data availability

Data used to generate Fig. 1b,d are available from the Gene Expression Omnibus under accession number GSE242156. MS data used to generate Fig. 3a, Extended Data Fig. 4a–d, Fig. 4a, Extended Data Fig. 7a–c, Extended Data Fig. 8a–c and Extended Data Fig. 6a are available from GlycoPOST under accession number GPST000467. MS data used to generate Extended Data Fig. 6b,c are available from GlycoPOST under accession number GPST000465. Replicate immunoblot and lectin blot data are available from the Texas Data Repository (https://doi.org/10.18738/T8/N9NF8B). Source data are provided with this paper.

References

81. Chakraberty, R., Reiz, B. & Cairo, C. W. Profiling of glycosphingolipids with SCDase digestion and HPLC-FLD–MS. *Anal. Biochem* **631**, 114361 (2021).
82. Doench, J. G. et al. Optimized sgRNA design to maximize activity and minimize off-target effects of CRISPR–Cas9. *Nat. Biotechnol.* **34**, 184–191 (2016).
83. Li, W. et al. MAGeCK enables robust identification of essential genes from genome-scale CRISPR/Cas9 knockout screens. *Genome Biol.* **15**, 554 (2014).
84. Liao, Y., Wang, J., Jaehnig, E. J., Shi, Z. & Zhang, B. WebGestalt 2019: gene set analysis toolkit with revamped UIs and APIs. *Nucleic Acids Res.* **47**, W199–W205 (2019).

85. Turner, S. D. qqman: an R package for visualizing GWAS results using Q–Q and Manhattan plots. *J. Open Source Softw.* **3**, 731 (2018).
86. Varadi, M. et al. AlphaFold Protein Structure Database: massively expanding the structural coverage of protein-sequence space with high-accuracy models. *Nucleic Acids Res.* **50**, D439–D444 (2022).
87. Kadirvelraj, R. et al. Comparison of human poly-*N*-acetyl-lactosamine synthase structure with GT-A fold glycosyltransferases supports a modular assembly of catalytic subsites. *J. Biol. Chem.* **296**, 100110 (2021).
88. Miller, J. J. et al. α-Galactosidase A-deficient rats accumulate glycosphingolipids and develop cardiorenal phenotypes of Fabry disease. *FASEB J.* **33**, 418–429 (2019).
89. Barone, A., Benktander, J., Teneberg, S. & Breimer, M. E. Characterization of acid and non-acid glycosphingolipids of porcine heart valve cusps as potential immune targets in biological heart valve grafts. *Xenotransplantation* **21**, 510–522 (2014).
90. Karlsson, H., Halim, A. & Teneberg, S. Differentiation of glycosphingolipid-derived glycan structural isomers by liquid chromatography/mass spectrometry. *Glycobiology* **20**, 1103–1116 (2010).
91. Shajahan, A., Heiss, C., Ishihara, M. & Azadi, P. Glycomic and glycoproteomic analysis of glycoproteins—a tutorial. *Anal. Bioanal. Chem.* **409**, 4483–4505 (2017).
92. Shajahan, A. et al. Comprehensive characterization of *N*- and *O*-glycosylation of SARS-CoV-2 human receptor angiotensin converting enzyme 2. *Glycobiology* **31**, 410–424 (2021).
93. Shajahan, A., Supekar, N. T., Gleinich, A. S. & Azadi, P. Deducing the *N*- and *O*-glycosylation profile of the spike protein of novel coronavirus SARS-CoV-2. *Glycobiology* **30**, 981–988 (2020).
94. Chai, W. et al. Negative-ion electrospray mass spectrometry of neutral underivatized oligosaccharides. *Anal. Chem.* **73**, 651–657 (2001).

Acknowledgements

We thank A. Singla, D. Andrade Silva and M. Burns for comments on the manuscript. We thank E. Capota and D. Andrade Silva for technical support. We thank A. Wands, D. Carroll, H. Wu, H. Khan and M. Shiloh for advice and reagents. We thank the UT Southwestern Proteomics Core Facility and its director, A. Lemoff. We acknowledge support from the National Institutes of Health (R01GM090271 and R35GM145599 to J.J.K. and R24GM137782 to P.A.), the Swedish Cancer Foundation (22 2079 Pj to S.T.) and the Welch Foundation (I-1686 to J.J.K.). M.T.G. received support from the NIH (T32GM145467). We thank C. Cairo (University of Alberta) for the RhtrECI plasmid and R. Schnaar (Johns Hopkins) for the P4 inhibitor.

Author contributions

A.C.G. and J.J.K. conceptualized the project and experimental approach, with input from A.B., R.S.R.K. and U.Y. A.C.G. conducted all cell culture experiments, flow cytometry experiments, functional assays and immunoblot experiments. A.B. prepared biotinylated CTB and CTB mutants with supervision from U.Y. S.A.A.-H. conducted MS analysis of intact glycolipids with supervision from P.A. M.T.G. performed MS analysis of procainamide-labeled glycans from glycolipids with supervision from P.A. D.Z. isolated neutral glycolipids and conducted MS analysis of their glycans with supervision from S.T. N.B.M. and S.A.A.-H. conducted *N*-linked and *O*-linked glycomic analyses with supervision from P.A. R.S.R.K. prepared EGCase and conducted preliminary analyses of glycolipids. X.Z. performed bioinformatics analyses with supervision from C.X. A.C.G. and J.J.K. wrote the manuscript with input from all authors.

Competing interests

The authors declare no competing interests.

Additional information

Extended data is available for this paper at https://doi.org/10.1038/s41589-024-01748-5.

Supplementary information The online version contains supplementary material available at https://doi.org/10.1038/s41589-024-01748-5.

Correspondence and requests for materials should be addressed to Jennifer J. Kohler.

Peer review information *Nature Chemical Biology* thanks the anonymous reviewers for their contribution to the peer review of this work.

https://doi.org/10.1038/s41589-024-01748-5

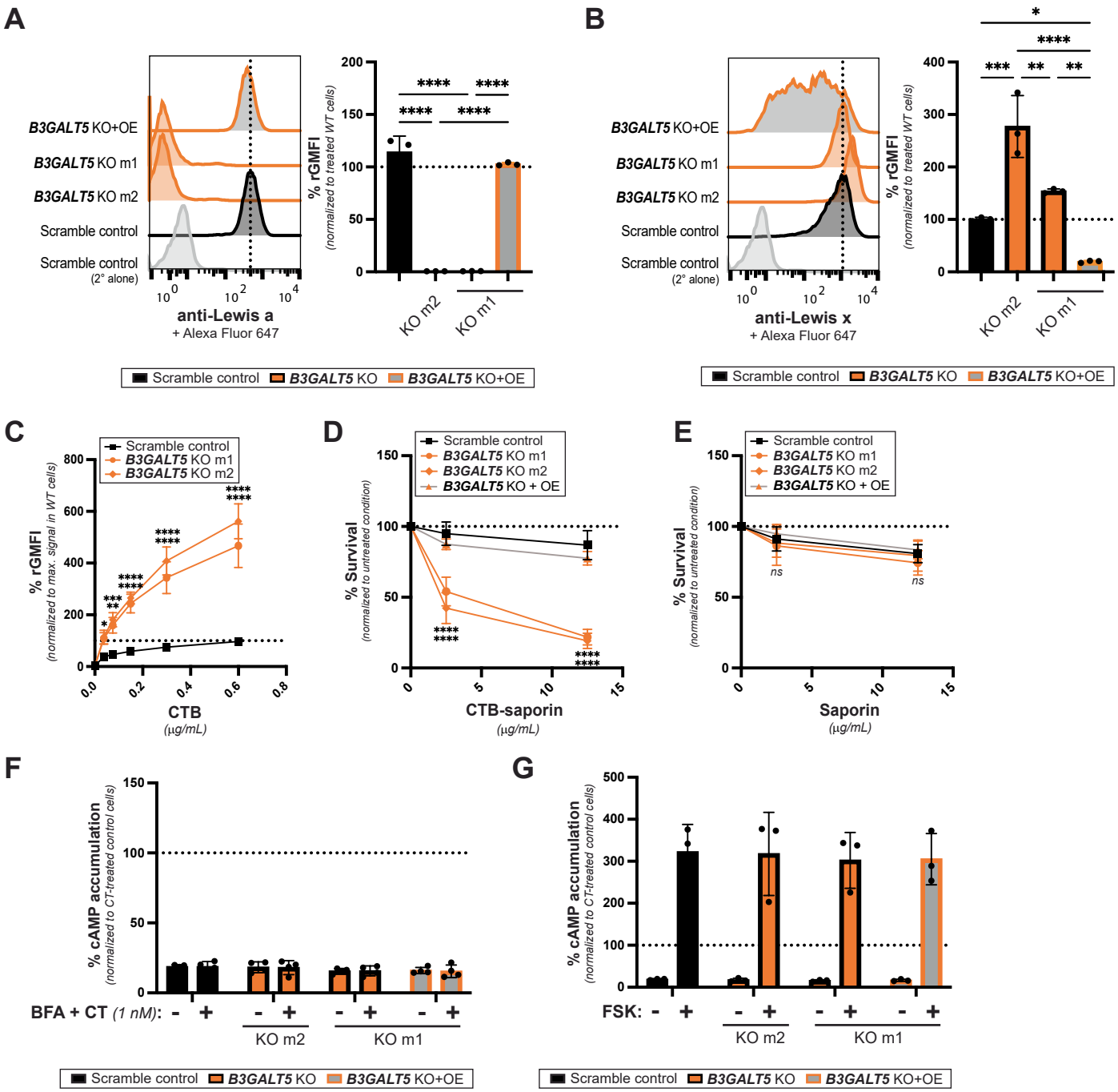

Extended Data Fig. 1 | Characterization of *B3GALT5*-KO and *B3GALT5*-KO + OE cells. (**A**, **B**) Representative histograms (left panel) from the flow cytometry analyses of cell surface binding of Lewis a antibody (**A**) or Lewis x antibody (**B**) to indicated cell lines. Bar graphs (right panel) show quantification from 3 independent trials. Error bars indicate mean ± SD. (**C**) Quantification of gMFI from flow cytometry analyses of cells treated with increasing concentrations of CTB. Data shown are from 3 independent trials and normalized to the maximum APC signal in WT cells. Error bars indicate mean ± SD. Indicated cell lines were incubated for 72 h with increasing concentrations of CTB-Saporin (**D**) or unconjugated saporin (**E**). Cell survival upon internalization of CTB-saporin was measured using the Cell Titer-Glo 2.0 assay. Data shown are luminescence values normalized to the signal from the untreated condition for each cell type. Each datapoint is a biological replicate consisting of 3 averaged technical replicates. Error bars indicate mean ± SD of 3 biological replicates. (**F**) Cells pretreated with BFA or vehicle control for 0.5 h were incubated for 1.5 h with CT (1 nM) or buffer alone. Accumulation of cAMP was measured. Data shown are inverse of luminescence values normalized first to the total amount of cells plated for each cell line, then to the signal in CT-treated control cells. Each datapoint is a biological replicate consisting of 3 averaged technical replicates. Error bars indicate mean ± SD of 3 biological replicates. (**G**) Control, *B3GALT5*-KO m1, m2 and KO + OE cells were treated with forskolin (10 µM) for 0.5 h and then analyzed as in panel F. Statistical analyses for panels A and B were performed by one-way ANOVA with Tukey correction and for panels **C**, **F**, and **G** by two-way ANOVA with Tukey correction.'ns' indicates not significant, **** indicates adjusted *P*-value < 0.0001. Exact *P*-values are as follows: 0.0004 and 0.0412 for control versus *B3GALT5*-KO m2 and *B3GALT5*-KO + OE; 0.0041 and 0.0024 for *B3GALT5*-KO m1 versus *B3GALT5*-KO m2 and *B3GALT5*-KO + OE, respectively (panel **B**); 0.0390 for control versus *B3GALT5*-KO m2 treated with 0.0375 µg/mL; 0.0002 and 0.0014 for control versus *B3GALT5*-KO m2 or m1 treated with 0.075 µg/mL, respectively (panel **C**).

https://doi.org/10.1038/s41589-024-01748-5

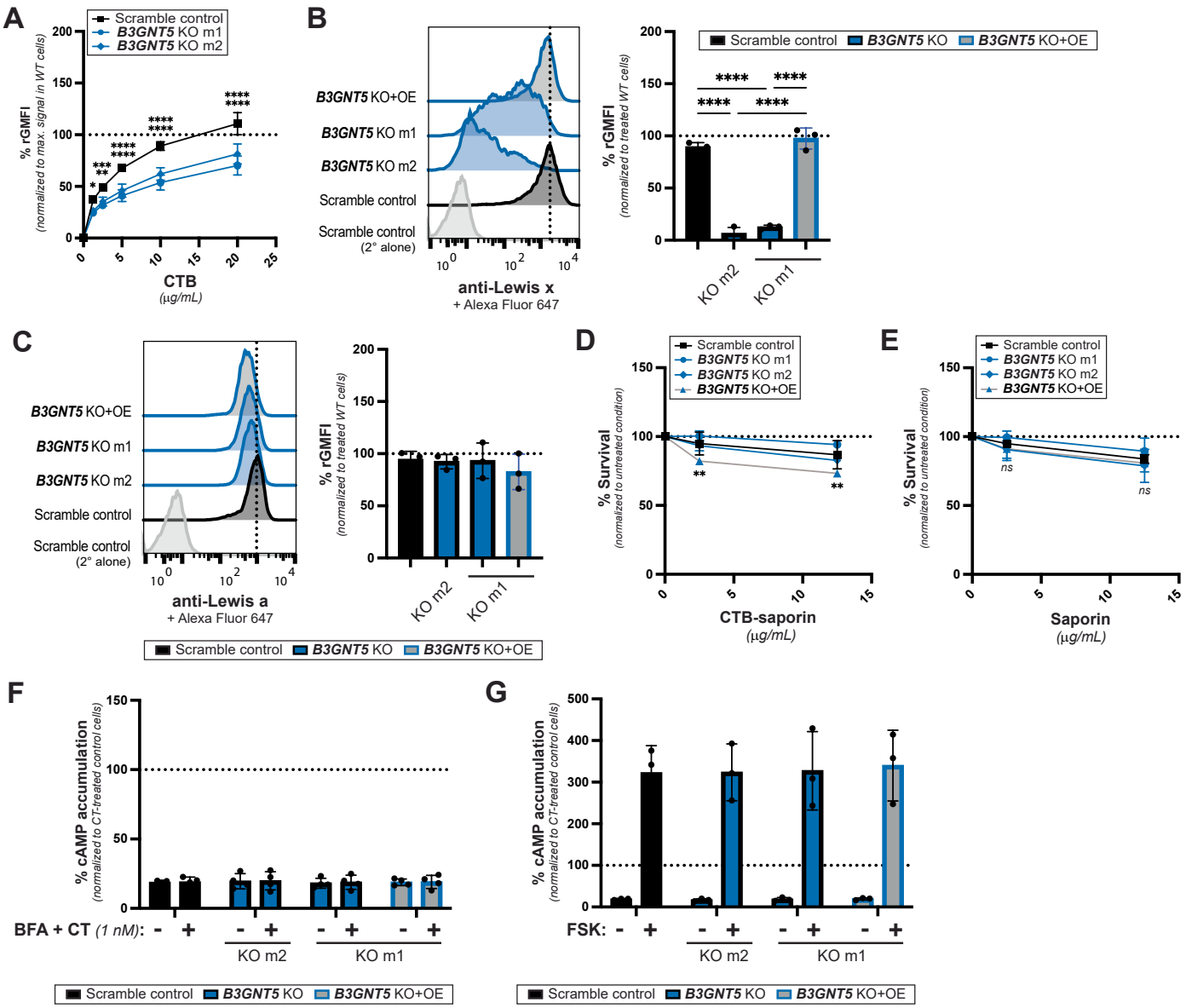

Extended Data Fig. 2 | Characterization of *B3GNT5*-KO and *B3GNT5*-KO + OE cells. (**A**) Quantification of gMFI from flow cytometry analyses of cells treated with increasing concentrations of CTB. Data shown are from 3 independent trials and normalized to the maximum APC signal in WT cells. Error bars indicate mean ± SD. (**B, C**) Representative histograms (left panel) from the flow cytometry analyses of cell surface binding of Lewis x antibody (**B**) or Lewis a antibody (**C**) to control, *B3GNT5*-KO m1, m2 and KO + OE cells. Bar graphs (right panel) show quantification from 3 independent trials. Control, *B3GNT5*-KO m1 and KO + OE cells were incubated for 72 h with increasing concentrations of CTB-Saporin (**D**) or unconjugated saporin (**E**). Cell survival upon internalization of CTB-saporin was measured using the Cell Titer-Glo 2.0 assay. Data shown are luminescence values normalized to the signal from the untreated condition for each cell type. Each datapoint is a biological replicate consisting of 3 averaged technical replicates. Error bars indicate mean ± SD of 3 biological replicates. (**F**) Cells pretreated with BFA or a vehicle control for 0.5 h were incubated for 1.5 h with CT (1 nM) or buffer alone. Accumulation of cAMP was measured. Data shown are inverse of luminescence values normalized first to the total amount of cells plated for each cell line, then to the signal in CT-treated control cells. Each datapoint is a biological replicate consisting of 3 averaged technical replicates. Error bars indicate mean ± SD of 3 biological replicates. (**G**) Control, *B3GNT5*-KO m1, m2 and KO + OE cells were treated with forskolin (10 μM) for 0.5 h and then analyzed as in panel F. Statistical analyses for panels **B** and **C** were performed by one-way ANOVA with Tukey correction and for panels **A**, **D**, **E**, **F**, and **G** by two-way ANOVA with Tukey correction. 'ns' indicates not significant, **** indicates adjusted *P*-value < 0.0001. Exact *P*-values are as follows: 0.0219 for control versus *B3GNT5*-KO m1 treated with 1.25 μg/mL; 0.0010 and 0.0077 for control versus *B3GNT5*-KO m1 or m2 treated with 2.5 μg/mL, respectively (panel **A**); 0.0059 and 0.0036 for control versus *B3GNT5*-KO + OE treated with 2.5 or 12.5 μg/mL CTB-saporin (panel **D**).

https://doi.org/10.1038/s41589-024-01748-5

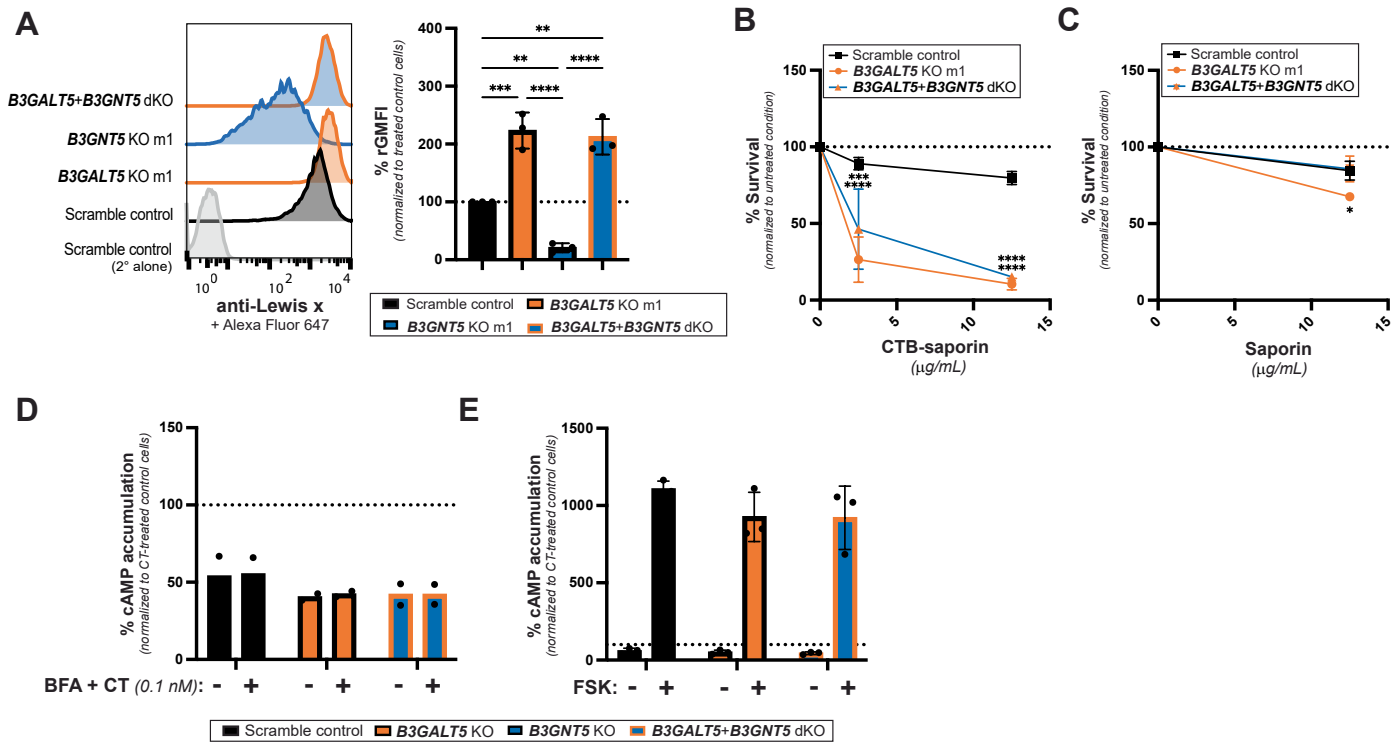

Extended Data Fig. 3 | Characterization of *B3GALT5* + *B3GNT5*-dKO cells. (**A**) Representative histograms (left panel) from the flow cytometry analyses of cell surface binding of Lewis x antibody to control, *B3GALT5* -KO m1, *B3GNT5*-KO m1, and *B3GALT5* + *B3GNT5*-dKO cells. Bar graph (right panel) shows quantification from 3 independent trials. (**B, C**) Control, *B3GALT5*-KO m1, and *B3GALT5* + *B3GNT5*-dKO cells were incubated for 72 h with increasing concentrations of CTB-Saporin (**B**) or unconjugated saporin (**C**). Cell survival upon internalization of CTB-saporin measured using the Cell Titer-Glo 2.0 assay. Data shown are luminescence values normalized to the signal from the untreated condition for each cell type. Each datapoint is a biological replicate consisting of 3 averaged technical replicates. Error bars indicate mean ± SD of 3 biological replicates. (**D**) Cells pretreated with BFA or a vehicle control for 0.5 h were incubated for 1.5 h with CT (1 nM) or buffer alone. Accumulation of cAMP was measured. Data shown are inverse of luminescence values normalized first to the total amount of cells plated for each cell line, then to the signal in CT-treated control cells. Each datapoint is a biological replicate (n = 2) consisting of 3 averaged technical replicates. (**E**) Control, *B3GALT5*-KO m1, m2 and KO + OE cells were treated with forskolin (10 µM) for 0.5 h and then analyzed as in panel **D**. Each datapoint is a biological replicate consisting of 3 averaged technical replicates. Error bars indicate mean ± SD of 3 biological replicates. Statistical analyses for panel **A** were performed by one-way ANOVA with Tukey correction and for panels **B**, **C**, **D**, and **E** by two-way ANOVA with Tukey correction. **** indicates adjusted *P*-value < 0.0001. Exact *P*-values are as follows: 0.0003 and 0.0048 for *B3GALT5* + *B3GNT5*-dKO versus control or *B3GALT5*-KO m1, respectively (panel **A**); 0.0002 and 0.0171 for control versus *B3GALT5* + *B3GNT5*-dKO treated with 2.5 µg/mL CTB saporin or 12.5 µg/mL saporin (panels **C** and **D**, respectively).

https://doi.org/10.1038/s41589-024-01748-5

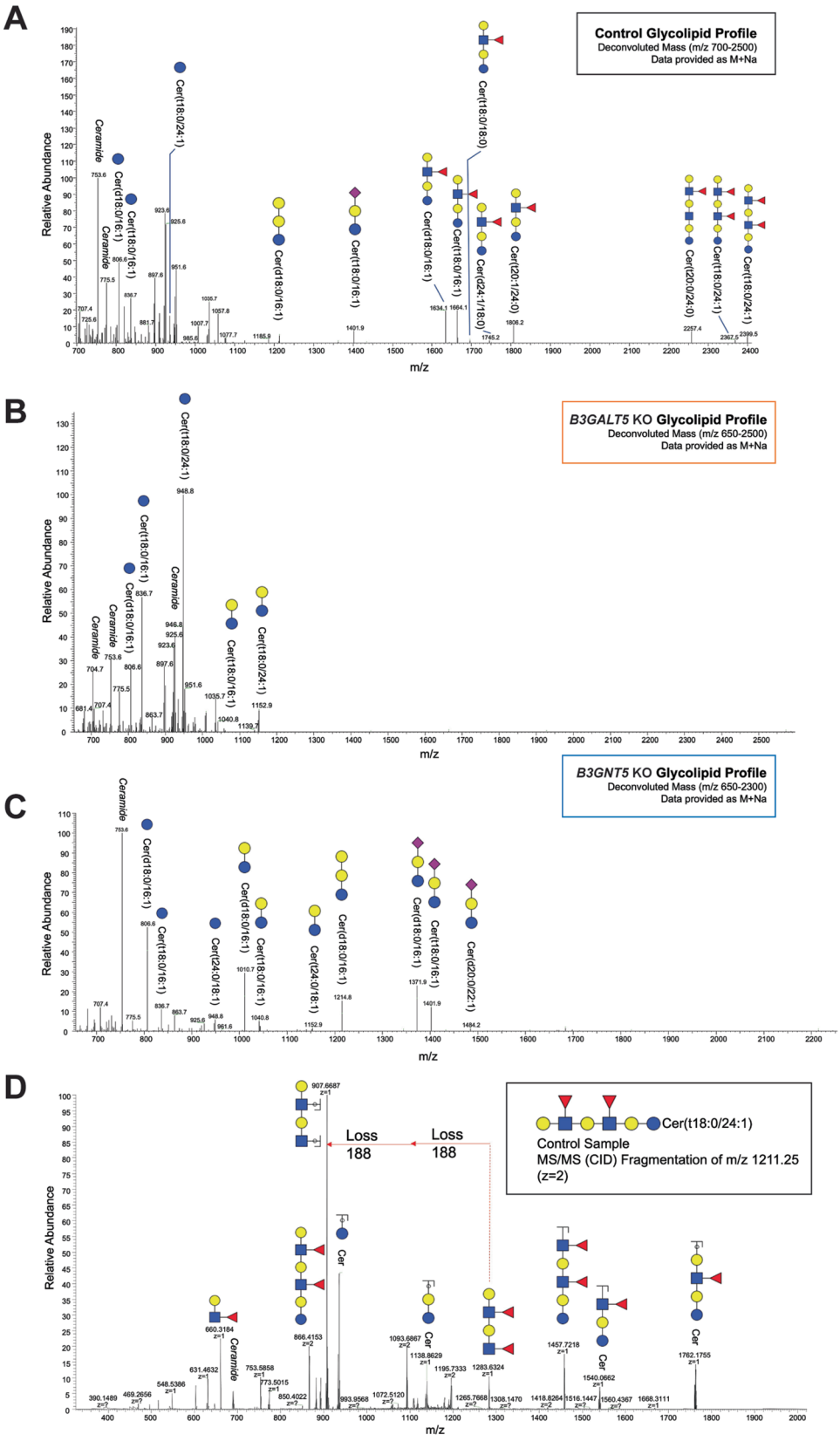

Extended Data Fig. 4 | Fucosylated lacto-series GSLs detected in control but not KO cell lines. MS analysis of GSLs from control (**A**), *B3GALT5*-KO m1 (**B**), and *B3GNT5*-KO m1 (**C**) cells. (**D**) Example MS/MS spectrum of a fucosylated lacto-series glycolipid detected in control cells, confirming structure.

https://doi.org/10.1038/s41589-024-01748-5

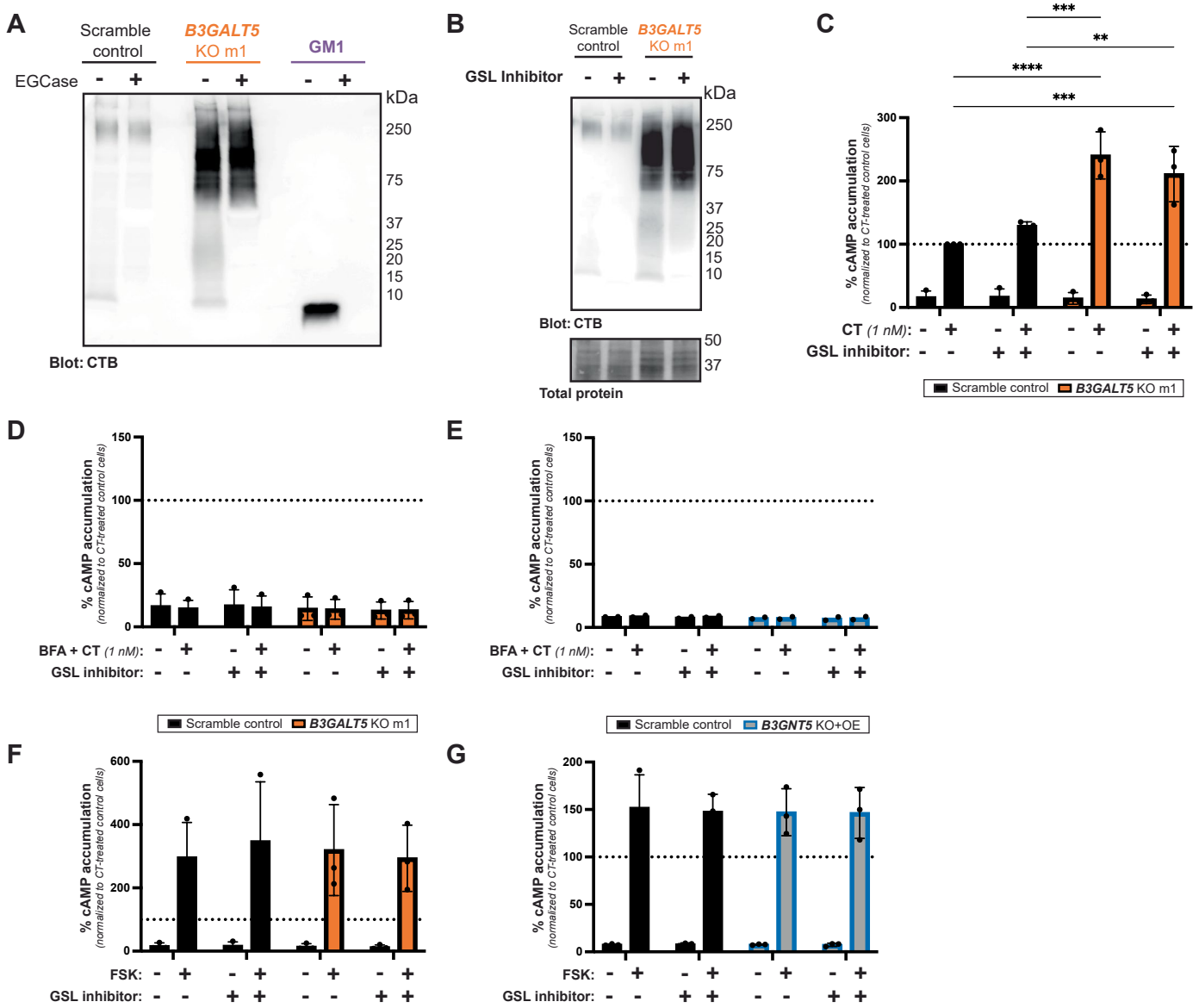

Extended Data Fig. 5 | Validation of GSLs as decoy receptors for CT. (**A**) Lectin blot with CTB-biotin of control and *B3GALT5*-KO m1 cell lysates, and pure GM1. Samples were treated for 16 h with endoglycoceramidase or a vehicle control. Data shown are a single representative trial of 3 independent biological replicates. (**B**-**G**) Control, *B3GNT5*-KO + OE, and *B3GALT5*-KO m1 cells were treated with P4 inhibitor of glycosphingolipid biosynthesis for 72 h then lysed for lectin blot analysis (**B**) or treated with BFA or a vehicle control for 0.5 h prior to incubation with CT (1 nM) for analysis of cAMP accumulation (**C**, **D**, and **E**). Alternately, cells were treated with forskolin (10 μM) for 0.5 h (**F** and **G**). Accumulation of cAMP was measured. Data shown are inverse of luminescence values normalized first to the total amount of cells plated for each cell line, then to the signal in CT-treated control cells. Each datapoint is a biological replicate (n = 2 in panel E, n = 3 in panels **C**, **D**, **F**, and **G**) consisting of 3 averaged technical replicates. Error bars indicate mean ± SD of 3 biological replicates. Statistical analyses were performed by two-way ANOVA with Tukey correction. Exact *P*-values are 0.0002 for control versus inhibitor-treated *B3GALT5*-KO m1 as well as inhibitor-treated control versus untreated *B3GALT5*-KO m1; for inhibitor-treated control versus inhibitor-treated *B3GALT5*-KO m1, the exact *P*-value is 0.0052 (panel **C**).

https://doi.org/10.1038/s41589-024-01748-5

A

Composition	Observed Mass	Retention Time	Percentage in *B3GALT5* KO	Percentage in *B3GNT5* KO+OE
Hex(2)	562.31	23.4	28.44	13.43
Hex(2)Fuc(1)	708.37	27.7	8.95	9.78
Hex(3)	724.38	29	40.33	45.83
Hex(2)HexNAc(1)	765.37	29.5	5.2	10.99
Hex(2)Sia(1)	853.42	30.6	8.2	3.53
Hex(2)HexNAc(1)Fuc(1)	911.43	34.8	0.53	0.59
Hex(3)HexNAc(1)	927.45	37.5	0.28	0.32
Hex(3)HexNAc(2)	1130.509	38.9	0.75	1.64
Hex(3)HexNAc(1)Fuc(1)	1073.49	39.9	1.75	0.79
Hex(4)HexNAc(1)	1089.48	41.1	1.73	4.26
Hex(4)HexNAc(1)Fuc(1)	1235.54	42	N.D.	Trace
Hex(3)HexNAc(1)Fuc(2)	1219.545	42.4	0.98	0.81
Hex(4)HexNAc(2)	1292.562	43.8	0.46	0.57
Hex(3)Fuc(1)	870.4078	45.9	0.52	0.19
Hex(4)HexNAc(2)Fuc(1)	1438.619	47.4	N.D.	Trace
Hex(4)HexNAc(2)Fuc(2)	1584.677	50.8	N.D.	0.55
Hex(2)HexNAc(1)Sia(1)	1056.44	52.5	1.66	4.71
Hex(3)HexNAc(2)Fuc(2)	1422.625	54.3	0.2	0.44
Hex(4)HexNAc(3)	1495.641	55.3	N.D.	1.57

B

m/z	Name	Structure	Diagn. ion (*m/z*)
503	Globotri	Gala4Galb4Glc	281
706	Globotetra	GalNAcb3Gala4Galb4Glc	484
706	Neolactotetra	Galb4GlcNAcb3Galb4Glc	281
852	Le^a penta	Galb3(Fuca4)GlcNAcb3Galb4Glc	348
852	Le^x penta	Galb4(Fuca3)GlcNAcb3Galb4Glc	364
868	Globopenta	Galb3GalNAcb3Gala4Galb4Glc	646
998	Le^b hexa	Fuca2Galb3(Fuca4)GlcNAcb3Galb4Glc	348
1071	Neolactohexa	Galb4GlcNAcb3Galb4GlcNAcb3Galb4Glc	646
1217	Le^a hepta	Galb3(Fuca4)GlcNAcb3Galb3/4GlcNAcb3Galb4Glc	348
1363	Le^a octa	Galb3(Fuca4)GlcNAcb3Galb3/4(Fuca3/4)GlcNAcb3Galb4Glc	348
754/ 1509	Le^b nona	Fuca2Galb3(Fuca4)GlcNAcb3Galb3/4(Fuca3/4)GlcNAcb3Gal b4Glc	348
864/ 1728	Le^a deca	Galb3(Fuca4)GlcNAcb3Galb3/4(Fuca3/4)GlcNAcb3Galb4Glc NAcb3Galb4Glc	348
864/ 1728	Le^x deca	Galb4(Fuca3)GlcNAcb3Galb3/4(Fuca3/4)GlcNAcb3Galb4Glc NAcb3Galb4Glc	364
937/ 1874	Le^x undeca	Galb4(Fuca3)GlcNAcb3Galb4(Fuca3)GlcNAcb3Galb4(Fuca3) GlcNAcb3Galb4Glc	364

C

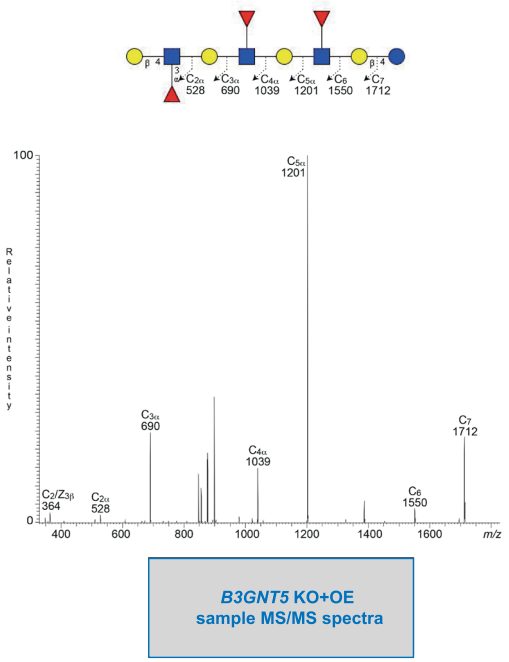

D

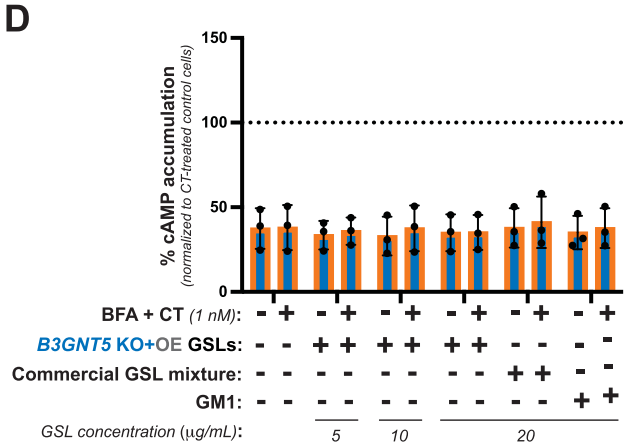

E

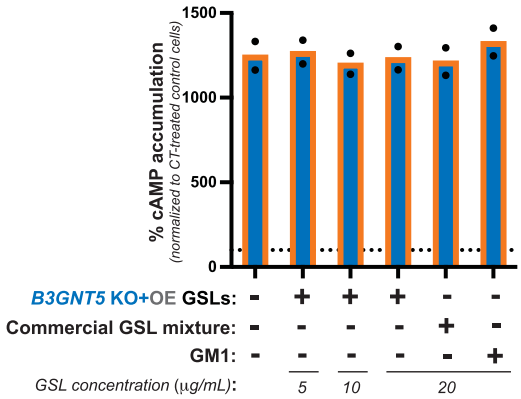

Extended Data Fig. 6 | Analysis of GSLs from *B3GNT5*-KO + OE cells. (**A**) Glycolipids were isolated from *B3GALT5*-KO m1 or *B3GNT5*-KO + OE cells. Glycans were released with endoglycoceramidase, labeled with procainamide, and analyzed by mass spectrometry with HILIC-FL separation. (**B, C**) LC-ESI/MS analysis of oligosaccharides obtained by digestion of neutral GSLs from *B3GNT5*-KO + OE cells with endoglycoceramidase I. Diagnostic ions indicate carbohydrate linkage positions. (**C**) An MS spectrum displaying a series of C type fragment ions ($C_{2\alpha}$ at *m/z* 528, $C_{3\alpha}$ at *m/z* 690, $C_{4\alpha}$ at *m/z* 1039, $C_{5\alpha}$ at *m/z* 1201, C_6 at *m/z* 1550, and C_7 at *m/z* 1712), which identified an oligosaccharide with Hex-(Fuc-)HexNAc-Hex-(Fuc-)HexNAc-Hex-(Fuc-)HexNAc-Hex-Hex sequence. The ion at *m/z* 364 is obtained by double glycosidic cleavage of the 3-linked branch ($C_2/Z_{3\beta}$), and characteristic for an internal 4-linked GlcNAc substituted with a Fuc at 3-position that is a terminal Le^x (refs. 90,94). Taken together this indicated an undecasaccharide with a terminal Le^x determinant. (**D, E**) *B3GALT5* + *B3GNT5*-dKO cells were incubated with GSLs extracted from *B3GNT5*-KO + OE cells, a commercial mixture of neutral GSLs, or purified GM1. Cells were then treated with BFA or a vehicle control for 0.5 h prior to incubation with CT (1 nM) for analysis of cAMP accumulation (**D**). Alternately, cells were treated with forskolin (10 μM) for 0.5 h (n = 2) (**E**). Accumulation of cAMP was measured. Data shown are inverse of luminescence values normalized first to the total amount of cells plated for each cell line, then to the signal in CT-treated control cells. Each datapoint is a biological replicate (n = 3 for panel **D**, n = 2 for panel **E**) consisting of 2 averaged technical replicates. Error bars indicate mean ± SD of 3 biological replicates (panel **D**). Statistical analyses were performed by two-way ANOVA with Tukey correction. No significant differences were observed.

https://doi.org/10.1038/s41589-024-01748-5

A

M+Na	Composition	Proposed Glycoform	Scramble Control *Average (±STDEV)*	*B3GALT5* KO *Average (±STDEV)*
1141.572	(Hex)2 (HexNAc)2 (Deoxyhexose)1		6.5% (±0.7%)	2.6% (±0.3%)
1171.583	(Hex)3 (HexNAc)2		1.6% (±0.1%)	0.9% (±0.1%)
1345.672	(Hex)3 (HexNAc)2 (Deoxyhexose)1		13.7% (±1.6%)	3.7% (±1.3%)
1375.683	(Hex)4 (HexNAc)2		2.6% (±0.2%)	1.1% (±0.8%)
1538.756	(Hex)6 (HexNAc)1		0.6% (±0.5%)	1.0% (±0.2%)
1579.783	(Hex)2 + (Man)3(GlcNAc)2		8.2% (±0.8%)	7.0% (±0.2%)
1590.798	(HexNAc)1 (Deoxyhexose)1 + (Man)3(GlcNAc)2		0.5% (±0.0%)	0.3% (±0.1%)
1742.854	(Hex)7 (HexNAc)1		0.6% (±0.1%)	0.5% (±0.4%)
1783.882	(Hex)3 + (Man)3(GlcNAc)2		17.5% (±1.4%)	15.4% (±3.8 %)
1835.924	(HexNAc)2 (Deoxyhexose)1 + (Man)3(GlcNAc)2		1.4% (±0.3%)	0.8% (±0.1%)
1946.954	(Hex)8 (HexNAc)1		0.7% (±0.2%)	1.0% (±0.2%)
1987.982	(Hex)4 + (Man)3(GlcNAc)2		8.4% (±0.5%)	10.5% (±0.5%)
2040.022	(Hex)1 (HexNAc)2 (Deoxyhexose)1 + (Man)3(GlcNAc)2		0.7% (±0.2%)	0.4% (±0.1%)
2070.029	(Hex)2 (HexNAc)2 + (Man)3(GlcNAc)2		0.7% (±0.1%)	1.2% (±0.1%)
2151.049	(Hex)9 (HexNAc)1		0.6% (±0.1%)	1.2% (±0.1%)
2156.073	(Hex)1 (HexNAc)1 (Deoxyhexose)1 (NeuAc)1 + (Man)3(GlcNAc)2		0.9% (±0.3%)	1.1% (±0.5%)
2192.081	(Hex)5 + (Man)3(GlcNAc)2		14.8% (±1.6%)	20.4% (±0.9%)
2203.097	(Hex)3 (HexNAc)1 (Deoxyhexose)1 + (Man)3(GlcNAc)2		1.1% (±0.0%)	0.8% (±0.1%)
2244.122	(Hex)2 (HexNAc)2 (Deoxyhexose)1 + (Man)3(GlcNAc)2		0.8% (±0.1%)	0.9% (±0.1%)
2274.135	(Hex)3 (HexNAc)2 + (Man)3(GlcNAc)2		0.6% (±0.1%)	0.7% (±0.3%)
2285.149	(Hex)1 (HexNAc)3 (Deoxyhexose)1 + (Man)3(GlcNAc)2		0.7% (±0.1%)	0.5% (±0.1%)
2390.182	(Hex)3 (HexNAc)1 (NeuAc)1 + (Man)3(GlcNAc)2		0.3% (±0.0%)	0.6% (±0.0%)
2396.181	(Hex)6 + (Man)3(GlcNAc)2		7.6% (±0.8%)	12.6% (±0.6%)
2401.194	(Hex)1 (HexNAc)2 (Deoxyhexose)1 (NeuAc)1 + (Man)3(GlcNAc)2		0.4% (±0.0%)	0.8% (±0.0%)
2418.209	(Hex)2 (HexNAc)2 (Deoxyhexose)2 + (Man)3(GlcNAc)2		0.5% (±0.1%)	0.6% (±0.1%)
2448.224	(Hex)3 (HexNAc)2 (Deoxyhexose)1 + (Man)3(GlcNAc)2		0.3% (±0.2%)	0.8% (±0.1%)
2459.238	(Hex)1 (HexNAc)3 (Deoxyhexose)2 + (Man)3(GlcNAc)2		0.5% (±0.1%)	0.6% (±0.1%)
2489.25	(Hex)2 (HexNAc)3 (Deoxyhexose)1 + (Man)3(GlcNAc)2		0.9% (±0.1%)	0.7% (±0.1%)
2592.304	(Hex)2 (HexNAc)2 (Deoxyhexose)3 + (Man)3(GlcNAc)2		0.5% (±0.1%)	0.6% (±0.0%)
2600.282	(Hex)7 + (Man)3(GlcNAc)2		1.1% (±0.1%)	1.7% (±0.0%)
2652.326	(Hex)4 (HexNAc)2 (Deoxyhexose)1 + (Man)3(GlcNAc)2		0.3% (±0.1%)	0.6% (±0.1%)
2663.337	(Hex)2 (HexNAc)3 (Deoxyhexose)2 + (Man)3(GlcNAc)2		1.1% (±0.2%)	1.2% (±0.2%)
2779.385	(Hex)2 (HexNAc)2 (Deoxyhexose)2 (NeuAc)1 + (Man)3(GlcNAc)2		0.2% (±0.1%)	0.4% (±0.0%)
2837.425	(Hex)2 (HexNAc)3 (Deoxyhexose)3 + (Man)3(GlcNAc)2		1.5% (±0.3%)	2.2% (±0.4%)
2850.421	(Hex)2 (HexNAc)3 (Deoxyhexose)1 (NeuAc)1 + (Man)3(GlcNAc)2		0.2% (±0.1%)	0.6% (±0.1%)
3024.511	(Hex)2 (HexNAc)3 (Deoxyhexose)2 (NeuAc)1 + (Man)3(GlcNAc)2		0.5% (±0.1%)	1.5% (±0.1%)
3198.601	(Hex)2 (HexNAc)3 (Deoxyhexose)3 (NeuAc)1 + (Man)3(GlcNAc)2		0.1% (±0.0%)	0.5% (±0.2%)
3215.613	(Hex)3 (HexNAc)3 (Deoxyhexose)4 + (Man)3(GlcNAc)2		0.2% (±0.0%)	0.3% (±0.0%)
3228.601	(Hex)3 (HexNAc)3 (Deoxyhexose)2 (NeuAc)1 + (Man)3(GlcNAc)2		0.3% (±0.1%)	1.2% (±0.7%)
3286.648	(Hex)3 (HexNAc)4 (Deoxyhexose)3 + (Man)3(GlcNAc)2		0.3% (±0.1%)	0.3% (±0.1%)

Note: Glycoforms shown represent only one of multiple possible isomers

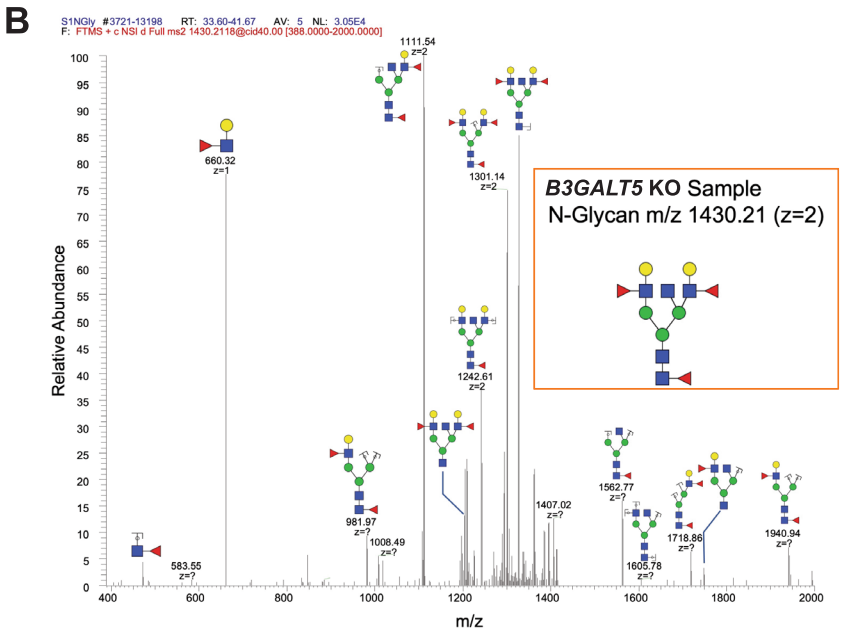

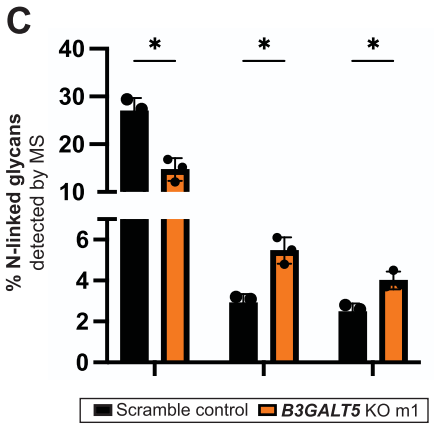

Extended Data Fig. 7 | See next page for caption.

https://doi.org/10.1038/s41589-024-01748-5

Extended Data Fig. 7 | *B3GALT5*-KO cells exhibit increased fucosylation on *N*-linked glycoproteins. (**A**) *N*-linked glycoforms detected in control and *B3GALT5*-KO m1 cells by LC-MS/MS analysis. Quantification is based on triplicate analysis. (**B**) Example MS/MS of a complex, fucosylated *N*-linked glycan detected in *B3GALT5*-KO m1 cells confirming placement of fucose. (**C**) Bar graphs showing the relative enrichment of mono- vs di- vs tri-fucosylated *N*-linked glycans detected by LC-MS/MS analysis of control and *B3GALT5*-KO m1 cells. Statistical analysis was performed by two-tailed t-test with Holm-Šídák correction. Exact adjusted *P*-value = 0.013508 for mono-fucosylated *N*-linked glycans detected in control versus *B3GALT5*-KO m1. Exact adjusted *P*-value = 0.014105 for both di- and tri-fucosylated *N*-linked glycans detected in *B3GALT5*-KO m1 versus control.

https://doi.org/10.1038/s41589-024-01748-5

A

M+Na	Composition	Proposed Glycoform	Scramble Control Average (±STDEV)	*B3GALT5* KO Average (±STDEV)
330.1887	$(HexNAc)_1$		19.7% (±1.0%)	0.9% (±0.3%)
534.2875	(Hex)1 (HexNAc)1		52.0% (±4.6%)	4.3% (±1.3%)
650.3345	(Hex)1 (NeuAc)1		2.8% (±1.6%)	3.7% (±0.9%)
779.4017	(Hex)1 (HexNAc)2		7.8% (±1.8%)	1.5% (±1.0%)
895.4597	(Hex)1 (HexNAc)1 (NeuAc)1		6.7% (±2.5%)	16.0% (±1.3%)
983.5113	(Hex)2 (HexNAc)2		10.1% (±2.2%)	3.4% (±1.3%)
1157.601	(Hex)2 (HexNAc)2 (Deoxyhexose)1		0.3% (±0.2%)	1.8% (±2.1%)
1256.634	(Hex)1 (HexNAc)1 (NeuAc)2		0.5% (±0.5%)	19.6% (±1.6%)
1344.685	(Hex)2 (HexNAc)2 (NeuAc)1		N.D.	6.9% (±0.3%)
1518.776	(Hex)2 (HexNAc)2 (Deoxyhexose)1 (NeuAc)1		N.D.	10.5% (±0.6%)
1606.829	(Hex)3 (HexNAc)3 (Deoxyhexose)1		N.D.	1.3% (±0.1%)
1705.861	(Hex)2 (HexNAc)2 (NeuAc)2		N.D.	2.2% (±0.1%)
1879.949	(Hex)2 (HexNAc)2 Deoxyhexose)1 (NeuAc)2		N.D.	14.1% (±1.6%)
1881.956	(Hex)4 (HexNAc)4		N.D.	7.2% (±0.9%)
1968.001	(Hex)3 (HexNAc)3 (Deoxyhexose)1 (NeuAc)1		N.D.	1.2% (±0.1%)
2142.091	(Hex)3 (HexNAc)3 (Deoxyhexose)2 (NeuAc)1		N.D.	1.9% (±0.1%)
2417.229	(Hex)4 (HexNAc)4 (Deoxyhexose)1 (NeuAc)1		N.D.	1.3% (±0.1%)
2503.265	(Hex)3 (HexNAc)3 (Deoxyhexose)2 (NeuAc)2		N.D.	2.3% (±0.3%)

Note: Glycoforms shown represent only one of multiple possible isomers

B

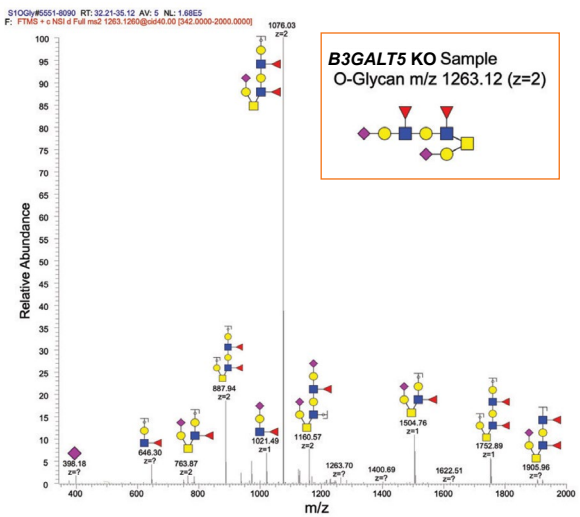

C

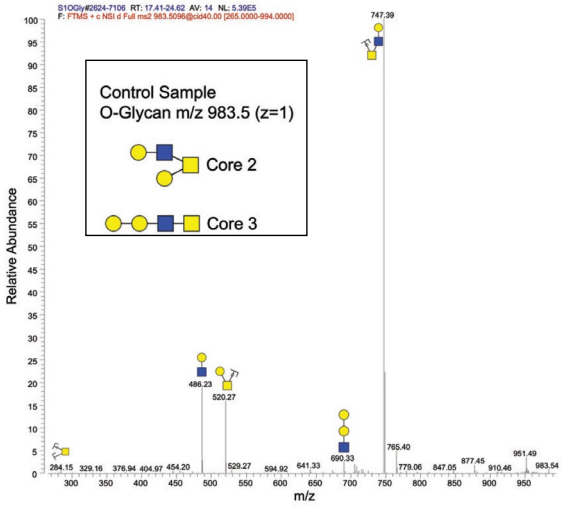

D

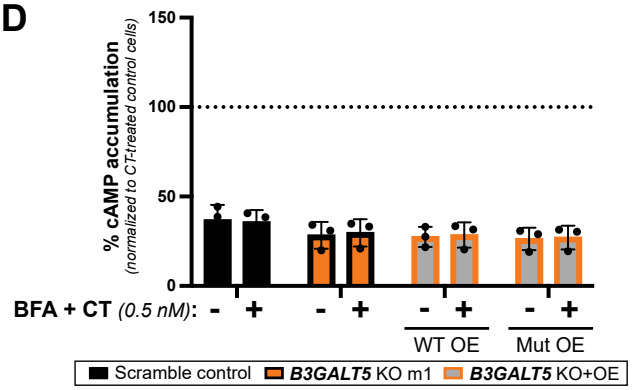

E

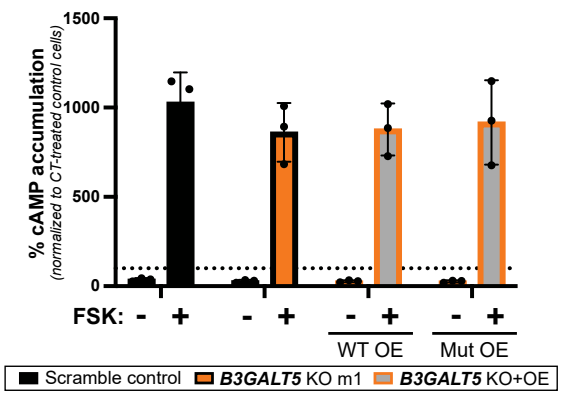

Extended Data Fig. 8 | *B3GALT5*-KO cells exhibit increased fucosylation on *O*-linked glycoproteins. (**A**) *O*-linked glycoforms detected in control and *B3GALT5*-KO m1 cells by LC-MS/MS analysis. Quantification is based on triplicate analysis. (**B**) Example MS/MS of a fucosylated *O*-linked glycan detected in *B3GALT5*-KO m1 cells. (**C**) Example MS/MS of core 2 *O*-linked glycan detected in *B3GALT5*-KO m1 cells confirming structure. (**D, E**) *B3GALT5*-KO m1 cells were rescued with either WT or catalytically dead (mut) *B3GALT5*-OE. Rescued cells were treated with BFA or a vehicle control for 0.5 h prior to incubation with CT (1 nM) for analysis of cAMP accumulation (**D**). Alternately, cells were treated with forskolin (10 µM) for 0.5 h (**E**). Accumulation of cAMP was measured. Data shown are inverse of luminescence values normalized first to the total amount of cells plated for each cell line, then to the signal in CT-treated control cells. Each datapoint is a biological replicate consisting of 2 averaged technical replicates. Error bars indicate mean ± SD of 3 biological replicates. Statistical analyses were performed by two-way ANOVA with Tukey correction. No significant differences were observed.

https://doi.org/10.1038/s41589-024-01748-5

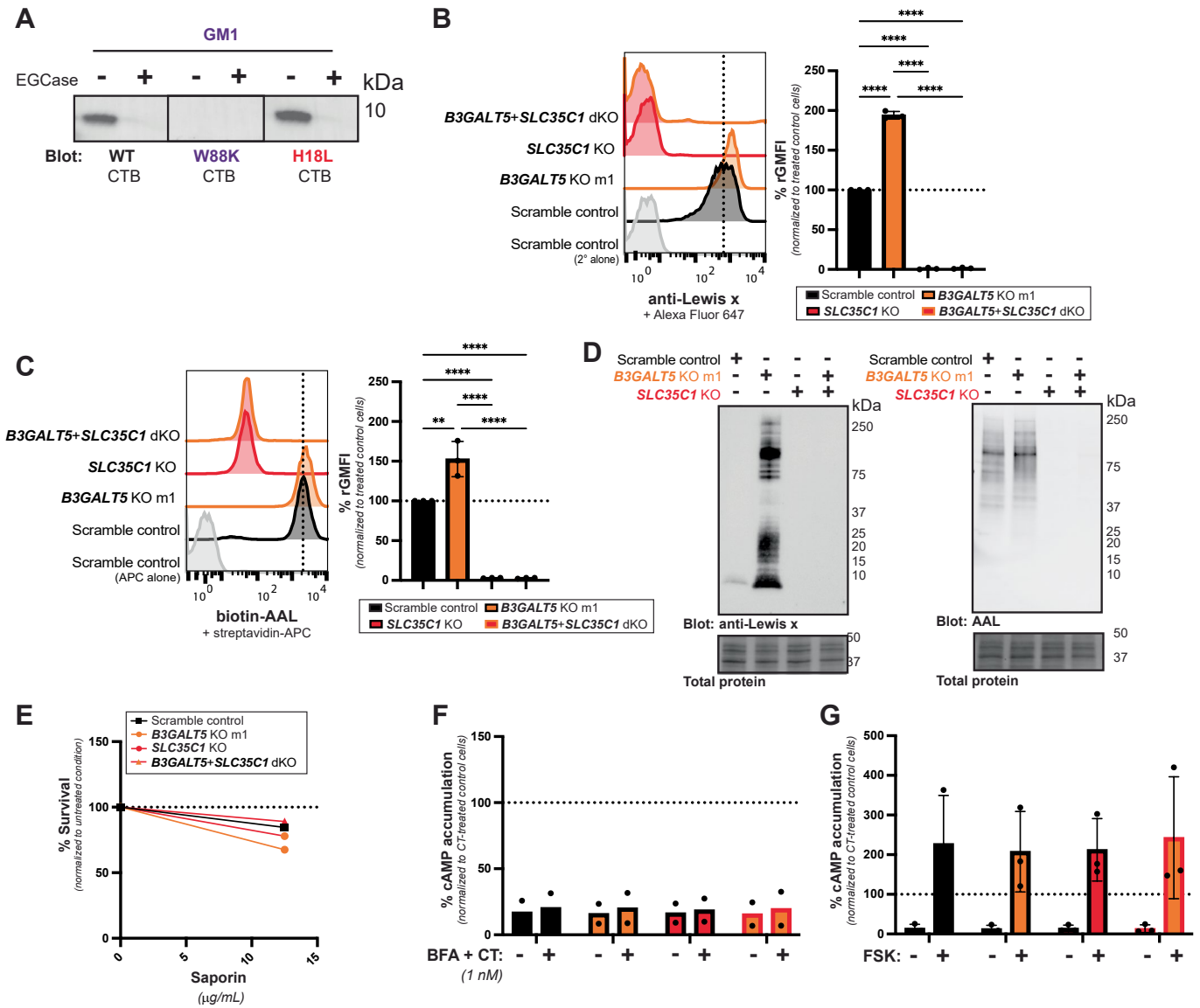

Extended Data Fig. 9 | Validation of *SLC35C1*-KO cell lines. (**A**) GM1 was treated with EGCase or vehicle, then detected by lectin blot using WT CTB-biotin, W88K CTB-biotin, and H18L CTB-biotin. Data presented are from 3 distinct membranes processed simultaneously (separated by vertical lines) and are a single representative trial from 3 biological replicates. (**B**, **C**) Representative histograms (left panel) from flow cytometry analyses of anti-Le^x antibody (**B**) and AAL (**C**) binding to surfaces of control, *B3GALT5*-KO m1, *SLC35C1*-KO, and *B3GALT5* + *SLC35C1*-dKO cells. Quantification of gMFIs (right panel) from 3 biological replicates are normalized to the maximum signal in control cells. Lysates from control, *B3GALT5*-KO m1, *SLC35C1*-KO and *B3GALT5* + *SLC35C1*-dKO cells were analyzed by immunoblot probing with anti-Le^x antibody or lectin blot probing with AAL (**D**). Data shown are a single representative trial from 3 biological replicates. (**E**) Control, *B3GALT5*-KO m1, *SLC35C1*-KO and *B3GALT5* + *SLC35C1*-dKO cells were incubated for 72 h with unconjugated saporin (12.5 μg/mL). Survival data shown are luminescence values normalized to the signal from the untreated condition for each cell type. Each datapoint indicates the mean of 2 biological replicates, each consisting of 3 averaged technical replicates. (**F**) Cells pretreated with BFA or a vehicle control for 0.5 h were incubated for 1.5 h with CT (1 nM) or buffer alone. Accumulation of cAMP was measured. Data shown are inverse of luminescence values normalized first to the total amount of cells plated for each cell line, then to the signal in CT-treated control cells. Each datapoint is a biological replicate (n = 2) consisting of 3 averaged technical replicates. (**G**) Cells were treated with forskolin (10 μM) for 0.5 h and then analyzed as in panel **F**. Each datapoint is a biological replicate consisting of 3 averaged technical replicates. Error bars indicate mean ± SD of 3 biological replicates. Statistical analyses were performed by one-way (panels **B** and **C**) or two-way (panels **F** and **G**) ANOVA with Tukey correction. **** indicates adjusted *P*-value < 0.0001. Exact *P*-value for control versus *B3GALT5*-KO m1 treated with AAL is 0.0018.

https://doi.org/10.1038/s41589-024-01748-5

A

Genes	Fold Change	*P*.Value
TCIRG1	4.93060497	0.00431572
LGALS9B	4.8689835	0.04142522
TRIM14	4.69438204	0.03076074
NT5E	4.68890403	0.01372595
ABCG2	4.64203619	0.00030817
ATP6V0A1	4.52403854	0.00289422
GPRC5A	4.48446607	0.03036069
CLRN3	4.47241346	0.00079488
FLOT1	**4.4043267**	**0.01611908**
LGALS9	4.40235264	0.25125444
ATP6V0C	4.31744057	0.00182088
ATP6V0A4	4.08058835	0.000876
MYADM	3.98437526	0.00543306
ABCC2	3.96403313	0.00690075
AQP1	3.9429867	0.03734743
STOM	3.81404742	0.00086234
DPEP1	3.50525402	0.00523696
SLC4A2	3.47380109	0.0007136
MAL2	3.44868984	0.03315269
ATP6V0A2	3.39373075	0.00423053
ATP6AP1	3.38889702	0.02707042
SLC4A7	3.37231139	0.00119136
EPB41L2	3.35853395	0.06796709
LMTK2	3.30078127	0.010185
LGALS3BP	3.24826492	0.01499782
LGALS8	3.22462499	0.03435593
PLPP2	3.21350217	0.00334389
FLOT2	3.06074302	0.01466696
LAMTOR1	3.05413787	0.0334058
BTBD9	3.04632155	0.02071636
ATP13A3	3.02902495	0.00231612
TRPM4	2.96610666	0.0147995
GALNT5	2.86666185	0.01205316
PIP4P1	2.85948864	0.02255006
MUC1	**2.85180235**	**0.04155424**
SLC12A6	2.82827641	0.00154035
ATP9A	2.80852553	0.00553872
SDCBP	2.78535281	0.0028892
TMED4	2.77459534	0.01247531
TPCN1	2.7485427	0.00841861
TMEM63A	2.74368581	0.0026814
ATP8B1	2.74308928	0.00442662
TNC	2.73625741	0.11865041
SLC6A6	2.71826597	0.02337299
PUSL1	2.70470513	0.14312872
EPS8L3	2.70234394	0.04098461
SLC12A9	2.63917179	0.00778633
KRT31	2.63081139	0.13983019
ANO1	2.62759478	0.00438845
KCNN4	2.61071996	0.01247144

B

GO Term	External ID	Adjusted *P*-Value
Apical Plasma Membrane	GO:0016324	0
Integral Component Of Plasma Membrane	GO:0005887	0
Plasma Membrane	GO:0005886	0
Integral Component Of Membrane	GO:0016021	3.5002E-08
ATP Hydrolysis Coupled Proton Transport	GO:0015991	6.4233E-07
Vacuolar Proton-Transporting V-Type Atpase, V0 Domain	GO:0000220	1.4871E-06
Transferrin Transport	GO:0033572	1.7246E-06
Vacuolar Proton-Transporting V-Type Atpase Complex	GO:0016471	8.7742E-06
Ion Transmembrane Transport	GO:0034220	1.7237E-05
Proton-Transporting Atpase Activity, Rotational Mechanism	GO:0046961	2.0854E-05
Phospholipid Translocation	GO:0045332	3.0193E-05
Lysosomal Membrane	GO:0005765	6.0917E-05
Specific Granule Membrane	GO:0035579	6.2556E-05
RNA Binding	GO:0003723	9.2646E-05
Phagosome Acidification	GO:0090383	0.00010742
Phagocytic Vesicle Membrane	GO:0030670	0.00012979
Tertiary Granule Membrane	GO:0070821	0.00014767
Insulin Receptor Signaling Pathway	GO:0008286	0.00016289
Vacuolar Acidification	GO:0007035	0.00127049
Vacuolar Proton-Transporting V-Type Atpase Complex Assembly	GO:0070072	0.00127049
Potassium Ion Transmembrane Transport	GO:0071805	0.00167169
Drug Transmembrane Transport	GO:0006855	0.00291416
Cell Volume Homeostasis	GO:0006884	0.00291416
Cytosol	GO:0005829	0.00296105
Potassium Ion Symporter Activity	GO:0022820	0.00510755
Potassium:Chloride Symporter Activity	GO:0015379	0.00510755

C

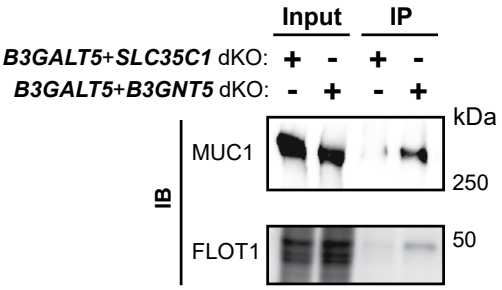

Extended Data Fig. 10 | See next page for caption.

https://doi.org/10.1038/s41589-024-01748-5

Extended Data Fig. 10 | CTB-interacting glycoproteins. (**A**) Top 50 proteins identified from CTB-biotin pulldown from *B3GALT5* + *B3GNT5*-dKO versus *B3GALT5* + *SLC35C1*-dKO cell lysates. Fold-change is the abundance in the *B3GALT5* + *B3GNT5*-dKO pulldown as compared to the *B3GALT5* + *SLC35C1*-dKO pulldown. Unadjusted *P*-values are derived from two-tailed student's t-test. (**B**) Gene ontology (GO) analysis using Fisher's exact test with Bonferroni correction to identify pathways enriched in CTB-biotin pulldown from *B3GALT5* + *B3GNT5*-dKO cell lysates as compared to *B3GALT5* + *SLC35C1*-dKO cell lysates. Top 25 pathways are shown. (**C**) Two hits (FLOT1 and MUC1, boldface font in panel **A**) were selected for confirmation. Total lysates and material from CTB-biotin pulldowns were analyzed by immunoblot using antibodies against FLOT1 and MUC1.

nature portfolio

Corresponding author(s): Jennifer Kohler

Last updated by author(s): August 28, 2024

Reporting Summary

Nature Portfolio wishes to improve the reproducibility of the work that we publish. This form provides structure for consistency and transparency in reporting. For further information on Nature Portfolio policies, see our Editorial Policies and the Editorial Policy Checklist.

Statistics

For all statistical analyses, confirm that the following items are present in the figure legend, table legend, main text, or Methods section.

n/a	Confirmed
☐	☒ The exact sample size (*n*) for each experimental group/condition, given as a discrete number and unit of measurement
☐	☒ A statement on whether measurements were taken from distinct samples or whether the same sample was measured repeatedly
☐	☒ The statistical test(s) used AND whether they are one- or two-sided *Only common tests should be described solely by name; describe more complex techniques in the Methods section.*
☒	☐ A description of all covariates tested
☐	☒ A description of any assumptions or corrections, such as tests of normality and adjustment for multiple comparisons
☐	☒ A full description of the statistical parameters including central tendency (e.g. means) or other basic estimates (e.g. regression coefficient) AND variation (e.g. standard deviation) or associated estimates of uncertainty (e.g. confidence intervals)
☐	☒ For null hypothesis testing, the test statistic (e.g. *F*, *t*, *r*) with confidence intervals, effect sizes, degrees of freedom and *P* value noted *Give P values as exact values whenever suitable.*
☒	☐ For Bayesian analysis, information on the choice of priors and Markov chain Monte Carlo settings
☒	☐ For hierarchical and complex designs, identification of the appropriate level for tests and full reporting of outcomes
☒	☐ Estimates of effect sizes (e.g. Cohen's *d*, Pearson's *r*), indicating how they were calculated

Our web collection on statistics for biologists contains articles on many of the points above.

Software and code

Policy information about availability of computer code

Data collection	Flow cytometry data were collected using CellQuest Pro version 6.0. Total protein staining of blots was imaged with ImageLab software (version 5.0) running on a ChemiDoc MP imager. Fluorescence imaging of blots was performed using control software for the Typhoon FLA 9500. Chemiluminescence imaging of blots was performed on a ChemiDoc MP imager running ImageLab Touch software version 2.3.0.07. Gen5 software (version 3.03) running on BioTek Synergy 2 microplate reader was used to collect luminescence and colorimetric data in 96-well plate format.
Data analysis	ImageLab Touch software version 2.3.0.07 was used for gel image analysis. Flow cytometry data were analyzed using FlowJo 10.9.0. Raw mass spectrometry data were manually interpreted with Thermo Xcalibur Qual Browser (versions 2.0.7 and 4.4) with structural assistance by GlycoWorkBench (version 1.2.4105). Statistical analysis of flow cytometry, CTB internalization data, and cAMP data was performed using GraphPad Prism versions 9 and 10.0.1. Proteomics data were analyzed using Proteome Discoverer 3.0. Analysis of mass spectrometry data for procainamide-labeled glycolipid glycans was performed with MassLynx v. 4.2

For manuscripts utilizing custom algorithms or software that are central to the research but not yet described in published literature, software must be made available to editors and reviewers. We strongly encourage code deposition in a community repository (e.g. GitHub). See the Nature Portfolio guidelines for submitting code & software for further information.

Data

Policy information about availability of data

All manuscripts must include a data availability statement. This statement should provide the following information, where applicable:

- Accession codes, unique identifiers, or web links for publicly available datasets
- A description of any restrictions on data availability
- For clinical datasets or third party data, please ensure that the statement adheres to our policy

Data used to generate Fig. 1B and 1D are available in the Gene Expression Omnibus database under accession number GSE242156. Mass spectrometry data used to generate Figure 3A, Extended Data Figure 4A, 4B, 4C, 4D, Figure 4A, Extended Data Figure 7A, 7B, 7C, Extended Data Figure 8A, 8B, 8C, and Extended Data Figure 6A are available at glycopost.glycosmos.org under accession number GPST000467. Mass spectrometry data used to generate Extended Data Figure 6B and 6C are available at glycopost.glycosmos.org under accession number GPST000465. Replicate immunoblot and lectin blot data are available in the online Texas Data Repository [doi.org/10.18738/T8/N9NF8B]. The proteomics analysis presented in Extended Data Figure 10A and B made use of the human protein database from UniProt available at uniprot.org.

Human research participants

Policy information about studies involving human research participants and Sex and Gender in Research.

Reporting on sex and gender	No human research participants were involved.
Population characteristics	No human research participants were involved.
Recruitment	No human research participants were involved.
Ethics oversight	No human research participants were involved.

Note that full information on the approval of the study protocol must also be provided in the manuscript.

Field-specific reporting

Please select the one below that is the best fit for your research. If you are not sure, read the appropriate sections before making your selection.

☒ Life sciences ☐ Behavioural & social sciences ☐ Ecological, evolutionary & environmental sciences

For a reference copy of the document with all sections, see nature.com/documents/nr-reporting-summary-flat.pdf

Life sciences study design

All studies must disclose on these points even when the disclosure is negative.

Sample size	No statistical methods were used to predetermine sample size. For immunoblots, triplicate or duplicate biological replicates were used. In our experience, when concordant results are obtained from this number of biological replicates, the outcome does not change if additional replicates are performed. Additionally, in many cases, observations made in early figure panels are further confirmed when similar samples are included in subsequent figure panels. For quantitative analysis, sample size was determined to be sufficient when a statistical comparison could be made to control samples (typically 3 unless prohibited by reagent availability). Sample sizes for each experiment are given in the figure legends.
Data exclusions	No data were excluded from the analyses.
Replication	For flow cytometry, blots (immunoblots and lectin blots), internalization assays, and cAMP assays, the number of replicates is indicated in the figure legend. Most experiments were performed in biological triplicate. The CRISPR screen was a single replicate. Rather than replicating the screen, we chose to validate the results by creating individual knockout cell lines. Glycomics analyses were performed in biological triplicate. Glycolipidomics analyses were single replicates, however we used three different methodological approaches to conduct glycolipidomics analysis with concordant results. All attempts at replication were successful.
Randomization	Randomization was not relevant to this study because there were no organisms or participants. All samples were treated identically.
Blinding	Blinding was not relevant because group allocation was not performed.

Reporting for specific materials, systems and methods

We require information from authors about some types of materials, experimental systems and methods used in many studies. Here, indicate whether each material, system or method listed is relevant to your study. If you are not sure if a list item applies to your research, read the appropriate section before selecting a response.

Materials & experimental systems

n/a	Involved in the study
☐	☒ Antibodies
☐	☒ Eukaryotic cell lines
☒	☐ Palaeontology and archaeology
☒	☐ Animals and other organisms
☒	☐ Clinical data
☒	☐ Dual use research of concern

Methods

n/a	Involved in the study
☒	☐ ChIP-seq
☐	☒ Flow cytometry
☒	☐ MRI-based neuroimaging

Antibodies

Antibodies used

Anti-beta subunit cholera toxin (Abcam, catalog no. ab 34992), lot numbers GR3279433 and GR3383904.
Anti-human CD15 clone HI98 [anti-Lewis x] (BD Biosciences, catalog no. 555400BD), lot numbers 7124624, 1313995, and 6033506.
Mouse-anti-human blood group Lewis a clone 7LE (Abcam, catalog no. ab3967).
Donkey anti-rabbit IgG Alexa Fluor® 647 (Abcam, ab150075), lot number GR3360238-2.
Goat anti-mouse IgM Alexa Fluor® 647 (Abcam, ab150123), lot number GR3296151-1
Goat anti-mouse IgG Alexa Fluor® 633 (Invitrogen, A-21050), lot number 56745A
goat anti-human FLOT1 (Thermo Fisher, catalog no. PA5-18053)
mouse anti-human MUC1, clone 214D4 (Sigma Aldrich, catalog no. 05-652)
donkey-anti goat IgG-HRP secondary antibody (Santa Cruz, catalog no. sc2020)
goat anti-mouse IgG-HRP secondary antibody (Invitrogen, catalog no. 31430)
goal anti-mouse igM-HRP secondary antibody (Invitrogen, catalog no. 31440)

Validation

The anti-beta subunit cholera toxin does not bind to the Colo205 cell lines if CTB is not included.
Anti-human CD15 clone HI98 recognition of anti-Lewis x is validated in PMC534418.
Mouse-anti-human blood group clone 7LE recognition of Lewis a is validated in PMC4223483.
Donkey Anti-Rabbit IgG H&L (Alexa Fluor® 647): https://www.abcam.com/en-us/products/secondary-antibodies/donkey-rabbit-igg-h-l-alexa-fluor-647-ab150075#
Goat Anti-Mouse IgM mu chain (Alexa Fluor® 647): https://www.abcam.com/en-us/products/secondary-antibodies/goat-mouse-igm-mu-chain-alexa-fluor-647-ab150123#
Goat anti-Mouse IgG (H+L) Cross-Adsorbed Secondary Antibody, Alexa Fluor™ 633: https://www.thermofisher.com/antibody/product/Goat-anti-Mouse-IgG-H-L-Cross-Adsorbed-Secondary-Antibody-Polyclonal/A-21050
Flotillin 1 Polyclonal Antibody: https://www.thermofisher.com/antibody/product/Flotillin-1-Antibody-Polyclonal/PA5-18053
mouse anti-human MUC1: PMID: 7698991
donkey-anti goat IgG-HRP secondary antibody: https://www.scbt.com/p/donkey-anti-goat-igg-hrp?srsltid=AfmBOopy74c60qKyhN2L5a4LbLv4UpxoyCOHBZ5g9Un2E_0YnBe0qqKh
goat anti-mouse IgG-HRP secondary antibodies: https://www.thermofisher.com/antibody/product/Goat-anti-Mouse-IgG-H-L-Secondary-Antibody-Polyclonal/31430
goat anti-mouse IgM-HRP secondary antibodies: https://www.thermofisher.com/antibody/product/Goat-anti-Mouse-IgM-Secondary-Antibody-Polyclonal/31440

Eukaryotic cell lines

Policy information about cell lines and Sex and Gender in Research

Cell line source(s)	Colo205 cells and HEK293T/17 are from the ATCC (CCL-222 and CRL-11268).
Authentication	Authentication was not performed.
Mycoplasma contamination	Cells tested negative for mycoplasma contamination.
Commonly misidentified lines (See ICLAC register)	Neither cell line is a commonly misidentified cell line.

Flow Cytometry

Plots

Confirm that:

☒ The axis labels state the marker and fluorochrome used (e.g. CD4-FITC).

☒ The axis scales are clearly visible. Include numbers along axes only for bottom left plot of group (a 'group' is an analysis of identical markers).

☒ All plots are contour plots with outliers or pseudocolor plots.

☒ A numerical value for number of cells or percentage (with statistics) is provided.

Methodology

Sample preparation	Media containing floating cells was collected and 2 mL of 10 mM EDTA in DPBS was added to adherent Colo205 cells and incubated for 5 min at 37 °C. Adherent cells were then dislodged by gentle resuspension and then combined with previously harvested floating cell population. Cells were washed twice by resuspending in DPBS, centrifuged at 500 g for 3 min and EDTA removed by aspiration. The cells were resuspended in DPBS containing 0.1 % (w/v) BSA (DPBS/BSA) and 3.5 x 10^5 cells were added per well to a V-bottom plate (Costar, catalog no. 3897). Cells were pelleted by centrifugation at 730 g for 5 min at 4 °C and washed twice by resuspension in 200 µL cold DPBS/BSA.
Instrument	BD FACSCalibur
Software	Data were collected with CellQuest Pro version 6.0 and analyzed with FlowJo 10.9.0.
Cell population abundance	For each sample, 10,000 gated events were collected.
Gating strategy	For all flow cytometry experiments, cells were gated based on forward scatter versus side scatter and dead cells were excluded by propidium iodide staining.

☒ Tick this box to confirm that a figure exemplifying the gating strategy is provided in the Supplementary Information.